Equatorial Kelvin Waves: A *UARS* MLS View*

PABLO O. CANZIANI AND JAMES R. HOLTON

Department of Atmospheric Sciences, University of Washington, Seattle, Washington

EVAN FISHBEIN, LUCIEN FROIDEVAUX, AND JOE W. WATERS

Jet Propulsion Laboratory, California Institute of Technology, Pasadena, California

(Manuscript received 21 March 1994, in final form 21 June 1994)

ABSTRACT

Data from the Microwave Limb Sounder instrument on the *Upper Atmosphere Research Satellite* are used to compare two periods of Kelvin wave activity during different stages of the equatorial quasi-biennial oscillation. The analysis is carried out using an asynoptic mapping technique. A wide bandpass filter is used to isolate the frequency bands where Kelvin waves have been identified in previous studies. Time–height and time–latitude plots of the bandpassed data are used to identify Kelvin wave activity in the temperature and ozone fields. Frequency spectra of temperature and ozone amplitudes are constructed to further analyze the latitudinal and meridional distribution of Kelvin wave activity in zonal wavenumbers 1 and 2. The characteristics identified in these plots agree well with theoretical predictions and previous observations of middle atmosphere Kelvin waves.

The time–height and time–latitude plots support the existence of Kelvin waves in discrete frequency bands; the slow, fast, and ultrafast Kelvin modes are all identified in the data. The characteristics of these modes do not vary much despite different mean flow conditions in the two periods examined.

For the Kelvin wave–induced perturbations in ozone, the change from a transport-dominated regime below 10 hPa to a photochemically controlled regime above 10 hPa is clearly apparent in the height dependence of the phase difference between temperature and ozone. The ratios of the ozone perturbation amplitude to the temperature perturbation amplitude for the various observed Kelvin wave modes are in agreement with model estimates and LIMS (Limb Infrared Monitor of the Stratosphere) observations in the lower half of the region sampled but appear to be too large in the upper stratosphere and lower mesosphere.

1. Introduction

Middle atmospheric Kelvin waves are eastward and vertically propagating equatorially trapped waves. They account for much of the large-scale variance in the equatorial stratosphere and lower mesosphere during the solstices. Vertically propagating atmospheric Kelvin waves were first described by Holton and Lindzen (1968); they have been the subject of numerous theoretical studies (e.g., Hayashi 1970; Holton 1970, 1972, 1973; Chang 1976; Boyd 1978a,b). The source of these waves appears to be forcing by unsteady convective heating in the tropical troposphere (Holton 1972; Salby and Garcia 1987), but this link has not been fully established from analysis of observations. Vertical transfer of westerly momentum by Kelvin waves provides a substantial portion of the westerly acceleration of the zonal mean flow in the quasi-biennial oscillation (QBO) of the equatorial lower stratosphere. Observed Kelvin waves are, however, apparently too weak to fully explain the westerly drive of the semiannual oscillation (SAO) (Hitchman and Leovy 1988) and may be insufficient to fully account for the westerly acceleration in the QBO (Takahashi and Boville 1992). It is now believed that momentum fluxes by mesoscale buoyancy waves are significant in the momentum budgets of the SAO and QBO.

According to linear theory (e.g., Holton 1992), in the absence of mean wind shear, Kelvin waves have a Gaussian structure in latitude, with maximum amplitude in zonal wind, temperature, vertical velocity, and pressure perturbations at the equator. There is no meridional wind perturbation associated with the linear Kelvin wave. In the longitude–height plane, Kelvin waves have the structure of buoyancy waves; they have downward and eastward phase propagation, which implies upward propagation of energy. The meridional and vertical scales of Kelvin waves are both simple functions of the intrinsic zonal phase speed, $\hat{c} = c - \bar{u}$, where c is the phase speed relative to the ground and $\bar{u}$ is the mean zonal wind speed. The e-folding de-

* Joint Institute for the Study of the Atmosphere and Oceans Contribution Number 259.

Corresponding author address: Dr. Pablo O. Canziani, Dept. of Atmospheric Sciences AK-40, University of Washington, Seattle, WA 98195.

cay width in latitude is $L_y = |a\hat{c}/\Omega|^{1/2}$ (where a is the radius of the earth and Ω its angular velocity of rotation); the vertical wavenumber is approximately $m = -N/\hat{c}$, where N is the buoyancy frequency and the negative sign indicates that vertical phase propagation is downward.

Observed Kelvin waves are of global scale in longitude. Most of their variance is found in zonal wavenumbers 1–3. They occur in three discrete speed ranges or, equivalently, frequency bands; these are defined as 1) "slow" (or Wallace–Kousky) waves (Wallace and Kousky 1968) with a phase speed range of 20–40 m s^{-1} and vertical wavelength of about 10 km; 2) "fast" waves (Hirota 1978), with a phase speed range 50–80 m s^{-1} and vertical wavelength of about 20 km; and 3) "ultrafast" waves (Salby et al. 1984), with a phase speed near 120 m s^{-1} and vertical wavelength of about 40 km.

Kelvin waves were first observed in the lower stratosphere from analysis of radiosonde data (Wallace and Kousky 1968; Maruyama 1969), and later in the upper stratosphere in rocketsondes (Hirota 1978) and satellite retrievals (Hirota 1979). The earliest satellite studies were carried out with nadir-viewing instruments, which have poor vertical resolution, so that only the longer vertical wavelengths could be detected. The advent of limb scanning remote sensing, beginning with the Limb Infrared Monitor of the Stratosphere (LIMS) onboard *Nimbus-7,* with its relatively good vertical resolution, led to important developments in the study of stratospheric Kelvin waves above the levels observed by radiosondes (Salby et al. 1984; Randel 1990; Salby et al. 1990).

Because the vertical velocity perturbations associated with Kelvin waves cause vertical displacements of material surfaces, vertically stratified long-lived tracer constituents should show variance correlated with Kelvin waves. Short-lived tracers whose concentrations are strongly temperature dependent should also show Kelvin wave associated variability. The oscillations observed in such tracers are referred to as Kelvin wave–induced oscillations. Randel (1990) and Salby et al. (1990) have studied the response of ozone and other tracers subjected to Kelvin wave activity, as observed during the LIMS experiment.

In Randel (1990) the temperature–ozone perturbation relationship was estimated from a simple linear model. The perturbation ozone mixing ratio μ' in this model is given by

$$\left(\frac{\partial}{\partial t} + \bar{u}\frac{\partial}{\partial x}\right)\mu' + w'\frac{\partial \bar{\mu}}{\partial z} = -\Gamma\mu' - \Theta T', \quad (1)$$

where $\partial\bar{\mu}/\partial z$ is the vertical gradient of the zonal mean mixing ratio, Γ is the photochemical relaxation rate, and Θ (K^{-1} s^{-1}) is the linearized ozone response coefficient to small temperature changes. The values of Γ and Θ come from the parameterization scheme described in Stolarski and Douglass (1985).

Equation (1) can be solved to yield relationships for the phase differences between μ' and T' and μ'/T' in terms of $\bar{\mu}_z$, Γ, and Θ. The solution shows that where ozone has a long lifetime, temperature and ozone perturbations are in phase, while in the upper stratosphere, where the chemical lifetime of ozone is short, the perturbations are in antiphase. Further details on the nature of Kelvin waves and their effect on tracers can be found in Salby et al. (1984), Randel (1990), and Salby et al. (1990).

The present effort extends the study of middle-atmospheric Kelvin waves to the first two years of observations by the Microwave Limb Sounder (MLS) on the *Upper Atmosphere Research Satellite* (*UARS*). The paper may be viewed as both a contribution to the validation of the MLS data and a documentation of Kelvin wave activity during the first two solstices of the *UARS* mission.

Previous limb measurements of the middle stratosphere were carried out with LIMS, which sensed atmospheric emissions in the infrared region of the spectrum. As its name indicates, MLS senses atmospheric emissions in the microwave region of the spectrum. Thus, the identification of Kelvin wave activity, which in comparison to mid- and high-latitude planetary waves typically has relatively small amplitudes and short vertical scales, serves as a check on the quality of the retrievals obtained with this technique. After establishing the existence of Kelvin wave signatures, the comparison of two separate solstice periods under different atmospheric conditions serves as a documentation of the variability of Kelvin wave activity during two subsequent solstices, which is possible for the first time with a limb scanning device.

In section 2 the data used and the method of data analysis are introduced. Because of limitations in the dataset (as discussed in section 2) a case study approach was used, which focused on the periods when Kelvin waves were strongest. The general character of the waves present during the selected periods is shown in section 3. Frequency spectra and various fields derived from the spectra for the periods of study are overviewed in section 4. In section 5 the relationship between temperature and ozone is analyzed, following Randel (1990). Throughout this paper the results obtained for MLS are compared to those obtained in similar studies of the LIMS observations. This does not mean the LIMS results are viewed as absolutes but rather as a general frame of reference. It must be pointed out that important discrepancies remain between the two versions of the LIMS database (V4 and V5) used in the above referenced papers.

2. Data and data analysis procedure

Temperature and ozone data obtained by MLS are used in the present study. These two variables are in-

dependently retrieved. Details of the instrument can be found in Barath et al. (1993), and the retrieval method is summarized in Waters et al. (1993). The data corresponds to the Level 3 AT, Version V0003, for both variables. The Level 3 AT data is archived along the trajectory of the limb view from the satellite at equal time intervals. The ozone retrieval is from the 205-GHz band of MLS. The height ranges, in the version used, are approximately 21–0.46 hPa and 46–0.2 hPa for temperature and ozone, respectively. In these height ranges the influence of a priori estimates is very small. MLS data are produced at all standard *UARS* pressure surfaces (approximately 3-km interval), but independent retrievals in the version available for this analysis are done on alternate *UARS* pressure surfaces. The data used in this research are from the 46.45-, 21.54-, 10-, 4.6-, 2.15-, 1-, 0.46-, and 0.22-hPa independent retrieval surfaces. The middle stratosphere and lower mesosphere are thus included in the present analysis, and the vertical spacing is of order 6–7 km, which means that the shortest resolvable vertical wavelength is of the order 12–14 km. Finally, the latitudinal limit imposed on the dataset is 28°N and 28°S, which corresponds to the region where there is nearly continuous temporal coverage. Poleward of 34° the *UARS* alternates between observing the Northern and Southern Hemisphere about every 26–40 days. This alternation between hemisphere views is a consequence of yaw maneuvers that are a necessity of the *UARS* mission, due both to instrumental and operational considerations. Because of edge effects in the analysis procedure described below the data between 28° and 34° were not considered. The yaw period imposes a stringent limit on the length of continuous time series available for analysis.

Any attempt to reconstruct a map directly from satellite data that have considerable variance in shorter periods will result in badly distorted fields due to the space–time coupling that is inherent to satellite measurements. For this reason the data analysis was carried out using the asynoptic mapping technique (Salby 1982a,b; Lait and Stanford 1988) with the modifications introduced in Elson and Froidevaux (1993). This method allows the retrieval of maps and spectra in a synoptic coordinate system, even though the actual measurements are asynoptic. This is an important consideration when a major part of the wave activity in the sample might occur at periods shorter than 5 days, as would be the case of the ultrafast waves and the diurnal tides present in the upper stratosphere and mesosphere.

Given the characteristics of the *UARS* orbit, all local times are covered in approximately 36 days when longitudinal coverage during both descending and ascending orbital phases is taken into account and the instrument whose data is being used has the capability to measure on both the day and night sides. Under these conditions the spectral analysis carried out during the asynoptic mapping procedure yields spectra that resolve zonal wavenumbers 1–6 and partially resolves wavenumber 7. The westward frequency range includes the diurnal component for wavenumber 1 only and somewhat lower frequencies for the remaining waves. For eastward propagating waves, the limiting period resolved by the method is close to 24 h for wavenumbers 1–5. The MLS temperature and ozone data are retrieved so as to satisfy the requirements of the method.

To generate the appropriate time series required for the mapping procedure, the level 3 AT data points were interpolated along the satellite track onto a uniform latitude grid, with a grid interval of 4° latitude centered about the equator. The regularly gridded time series can then be separated into time series for descending and ascending nodes at each latitude, as required by the method. These time series are then transformed using a standard fast Fourier transform (FFT). In this particular case the first and last 10% of each series was tapered using a cosine window before application of the FFT. When combined node data are used, this method makes it possible to obtain twice-daily synoptic maps. Further information regarding the behavior of the spectral limits for the method and other technical details can be found in Salby (1982a), Lait and Stanford (1988), and Elson and Froidevaux (1993). In subsequent sections of this paper, reconstructed time–height plots, time–latitude plots, and frequency spectra will be shown.

As previously mentioned, the wavenumber spectra of Kelvin waves are characteristically red. In the current study we have limited ourselves to zonal wavenumbers 1 and 2, where most of the Kelvin wave variance appears to be concentrated, as has been the case for previous datasets. As clearly pointed out by Salby et al. (1984), given the episodic behavior of Kelvin wave events, the frequency spectra must be viewed as an average statistic of the sampled period. Because of the nonstationary nature of the waves, the variance of a given component might be smeared over the neighboring frequencies. As a consequence, the amplitudes observed in the spectra are bound to be much smaller than the actual amplitude reached by a Kelvin wave during a given event.

The coherency studies of temperature and ozone in section 5 were carried out using the procedures described in Randel (1990). In the present case, however, because of the yaw maneuvers every 30–40 days, which do not allow for a sufficiently long and continuous time series, two or more spectra from successive yaws were averaged and then smoothed in frequency with a triangular 1–2–1 filter. When two spectra were used, this gave the order of 10 degrees of freedom. This yields reasonable values for the confidence levels of the coherency squared.

Two sample periods will be discussed. The first starts on 6 December 1991 (*UARS* day 86, or UD86 for short) and lasts through 13 February 1992 (UD155),

which hereafter will be referred to as "period I." The second sample (period II) starts on 18 July 1992 (UD311) and lasts through 20 September 1992 (UD375). Thus, both solstices of the first year of the *UARS* mission are considered. Hirota (1978) using rocket observations and Randel and Gille (1991) using Solar Backscatter Ultraviolet (SBUV) observations showed that Kelvin waves are predominant during the solstice seasons and that the Kelvin wave variance is greater after the December solstice than after the June solstice. In the case of the second sampling period, though it would have been better to start the time series at a date much closer to the actual solstice, this was not possible due to operational problems on the satellite, which resulted in some problems in the spacing of the data during late June and early July.

The zonal mean zonal wind averaged over each of the sampled periods can be seen in Fig. 1. These plots have been obtained using the winds from the U.K. Meteorological Office (UKMO) data assimilation model (Swinbank and O'Neill 1994), provided as correlative data product for the *UARS* database. Negative values correspond to easterly flows, while positive values show westerly flows. Figure 1a shows that period I corresponds to the easterly phase of the QBO, while Fig. 1b shows that period II corresponds to the onset of the westerly phase. During period I, between 8°S and 8°N (in the region between 50 and 20 hPa), there is an easterly vertical shear of the order of 2.5 m s^{-1} km^{-1}, and above 10 hPa there is a narrow region, mostly north of the equator, with far weaker westerly shear. The period of the LIMS experiment in 1979 corresponded to the easterly phase of the QBO, though the winds inferred from LIMS temperatures between 30 and 1 hPa were almost twice as strong as during period I of our analysis. Furthermore, according to Hitchman and Leovy (1988), there was a descending layer with a strong westerly shear in the vicinity of 1–3 hPa during the LIMS experiment. Despite these differences, the similarities in the global flow patterns between the winter solstice described in the LIMS studies and that described for period I allow for a close comparison of the MLS and LIMS observations.

On the other hand, during period II, the region between 40 and 20 hPa in the vicinity of the equator shows a westerly vertical shear of the order of 3–4 m s^{-1} km^{-1}. Above 20 hPa there is a region of easterly shear, which becomes quite weak above 5 hPa. This wind distribution implies that vertically propagating Kelvin waves face two very different zonal flow regimes. According to Holton (1970) and the LIMS results from Salby et al. (1984), for a particular wave mode increasing westerly flow will result in a reduction of the intrinsic phase speed, a shortening of the vertical wavelength, and a reduction in the latitudinal extent. These tendencies are particularly apparent for the slower, shorter vertical wavelength oscillations, although they should not be significant for the fast and ultrafast Kelvin modes (see Table 1). The reduction in intrinsic phase speed will also increase the radiative and mechanical damping rates and hence reduce the amplitude of the mode as it propagates upward. In an east-

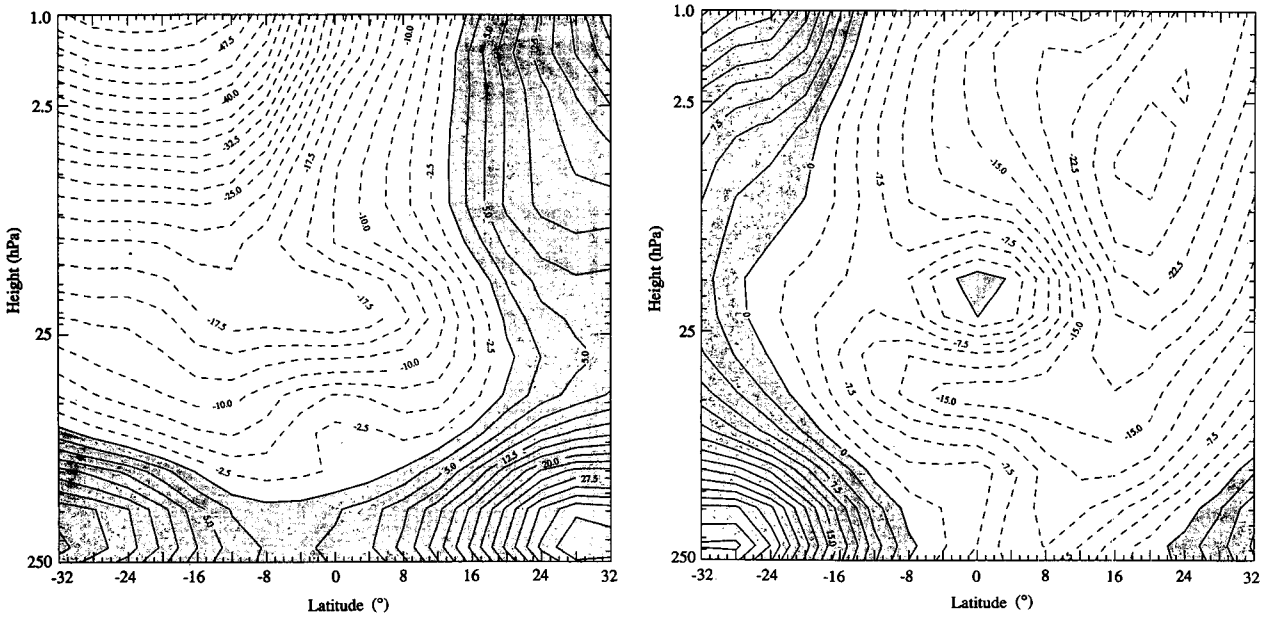

FIG. 1. Meridional cross section of the mean zonal flow (m s^{-1}) averaged in time over the length of each period under study: (a) period I; (b) period II. The area shaded in gray corresponds to the westerly flow, and dashed contour lines to easterly flow. (Contour interval is 2.5 m s^{-1}.)

TABLE 1. Some properties of Kelvin waves detected in MLS temperature and ozone fields.

Sample period	Zonal wavenumber	Zonal phase speed (m s^{-1})	Observed period (days)	Intrinsic period (days) at various altitudes				Vertical wavelength (km)
				20 hPa	10 hPa	5 hPa	1 hPa	
I	1	57.9	8.0	6.0	6.6	6.5	5.6	20
I	1	115.8	4.0	3.4	3.6	3.6	3.3	44
I	2	38.6	6.0	4.0	4.5	4.5	3.6	14
I	2	57.9	4.0	3.0	3.3	3.3	2.8	20
II	1	66.2	7.0	7.0	6.3	5.8	5.9	20
II	1	102.9	4.5	4.5	4.2	4.0	4.1	30
II	2	29.0	8.0	8.0	6.4	5.4	5.5	14
II	2	57.9	4.0	4.0	3.6	3.2	3.3	20

erly flow, on the other hand, the vertical wavelength of the Kelvin mode is increased and the amplitude and latitudinal extent are enhanced as it propagates upward. Thus, in principle, the slower modes should be present during period I, while during period II their amplitudes should be reduced and they should show a decrease in latitudinal extent in the westerly shear zone.

3. Evidence for Kelvin wave activity in the temperature fields

Evidence for Kelvin wave activity was first sought in twice-daily synoptic maps created using the technique described above. These maps were produced by summing wavenumbers 1–4 and removing the daily zonal mean and variability at frequencies higher than 0.5 cycles per day. This is a reasonable procedure since most of the variance is in the first three wavenumbers and the higher frequencies include tidal features, which tend to obscure the slower-moving waves.

From these maps equatorial time–longitude plots at the 1-hPa surface and time–height plots at 0° longitude were obtained. Figure 2 shows examples of the resulting plots for temperature and ozone for period II. These and the set of plots that follow are obtained by compositing time–height and latitude–height plots for successive sampling periods of *UARS* so as to fully map the periods under study. The gaps in the plot are the result of the yaw maneuvers and the fact that the first and last two half-day plots obtained from the asynoptic mapping must be discarded due to their proximity to the edge of the sampling window. Each section of the plot is an independent evaluation. The episodic eastward-propagating oscillations are the main feature in the time–longitude sections (Figs. 2c,d). In the time–height plots (Figs. 2a,b) descending phase lines are clearly apparent. Another interesting feature is the strong anticorrelation between the ozone and temperature fields, which can be seen in the time–longitude plots and above approximately 10 hPa in the time–height plots. Though the correlation is not perfect, this result is consistent with the short photochemical lifetime of ozone in the equatorial upper stratosphere and the known temperature dependence of ozone photochemistry.

The behavior of individual zonal wavenumbers in specific frequency bands is next examined to observe the evolution of the eastward-propagating modes. Table 1 shows the zonal phase speeds and observed periods for the dominant modes in each sample period. Also shown in the table are the intrinsic (Doppler shifted) periods at various heights. The structure of these various modes can be examined by constructing time–height and time–latitude plots for specific zonal wavenumbers and frequency bands. An example is shown in Fig. 3 for zonal wavenumber 1 in the temperature field during period I. The frequency band plotted corresponds to periods between 20 and 5.5 days. This band includes the slower Wallace–Kousky waves typically present in the lower stratosphere and the fast Kelvin waves with periods between 6 and 10 days, which, from LIMS data, appear to be a dominant feature of the equatorial middle atmosphere during the solstice. The dominant feature in Fig. 3a, which shows a time–height plot of temperature at the equator and 0° longitude, is a wave with descending phase and a period in the vicinity of 8 days. The estimated vertical wavelength is of the order of 20 km, and the horizontal phase speed is of the order of 58 m s^{-1}. The amplitude varies at all height ranges throughout the duration of the sample. For example, the largest amplitudes at 1 hPa are reached near the beginning and toward the end of this sample. This amplitude variation appears to be associated with the upward propagation of discrete "wave packets," a term first used in Coy and Hitchman (1984). There appear to be at least three successive wave packets propagating from the lower to the upper limits of the plots in quick succession. The peak to peak range reached during active periods can be of the order of 4°C.

Figure 3b, a time–latitude section at 1 hPa for longitude 0°, shows that the dominant oscillation is indeed an equatorially trapped mode. The latitudinal extent at 1 hPa, as measured in degrees between the north and south quarter-power points, varies between 42° and 24° (the former is consistent with linear Kelvin wave the-

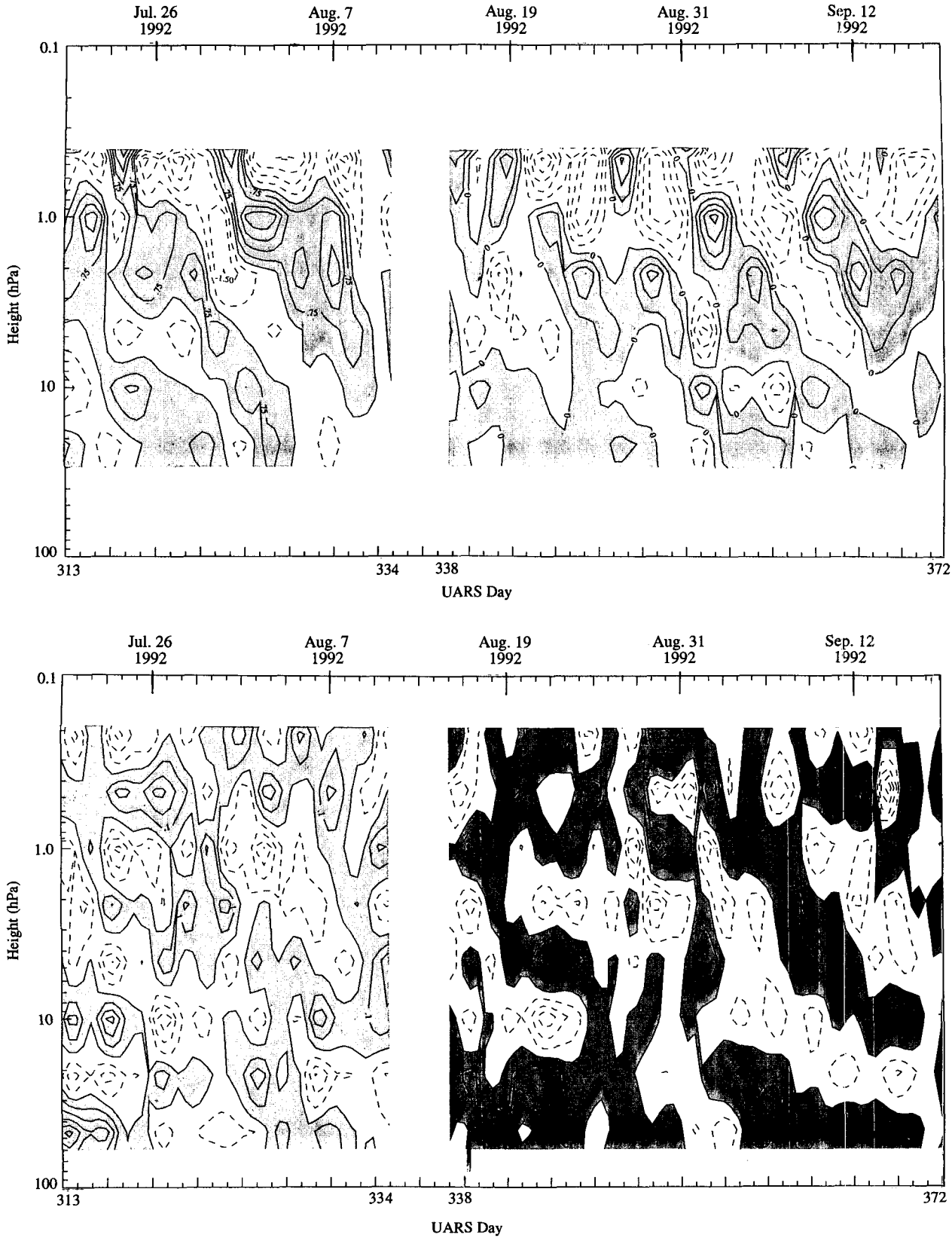

FIG. 2. Time–height and time–longitude plots of temperature [(a), (c)] and ozone [(b), (d)] fields at the equator during period II. The mean zonal fields and the high-frequency oscillations have been removed. The time–height plot is for 0° longitude and the time–longitude plot is on the 1-hPa surface. Positive amplitudes are shaded in gray. Note the anticorrelation between temperature and ozone visible in the upper stratosphere. Temperature contours are given every 0.75°C, and ozone mixing ratio contours every 0.1 ppmv.

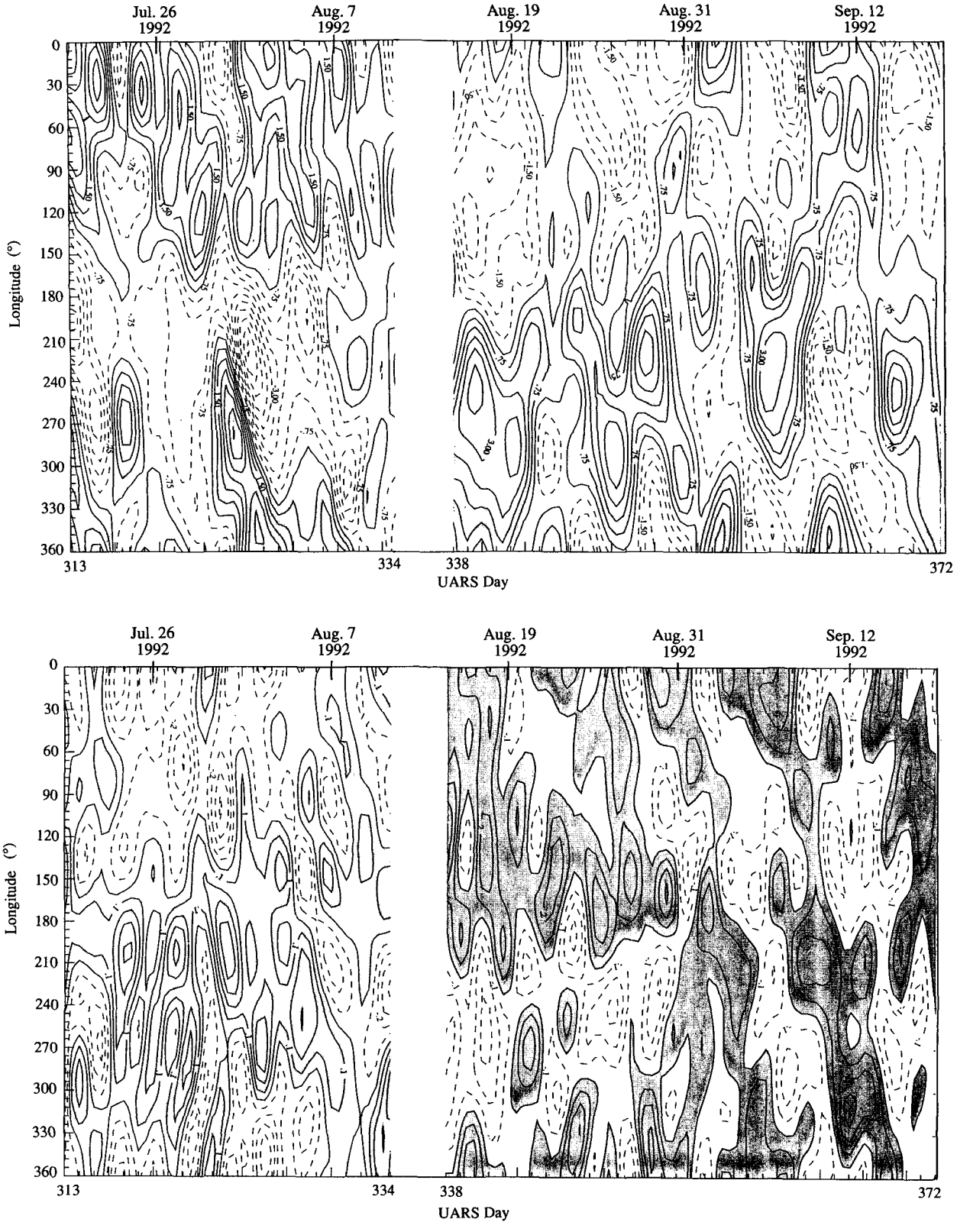

FIG. 2. (*Continued*)

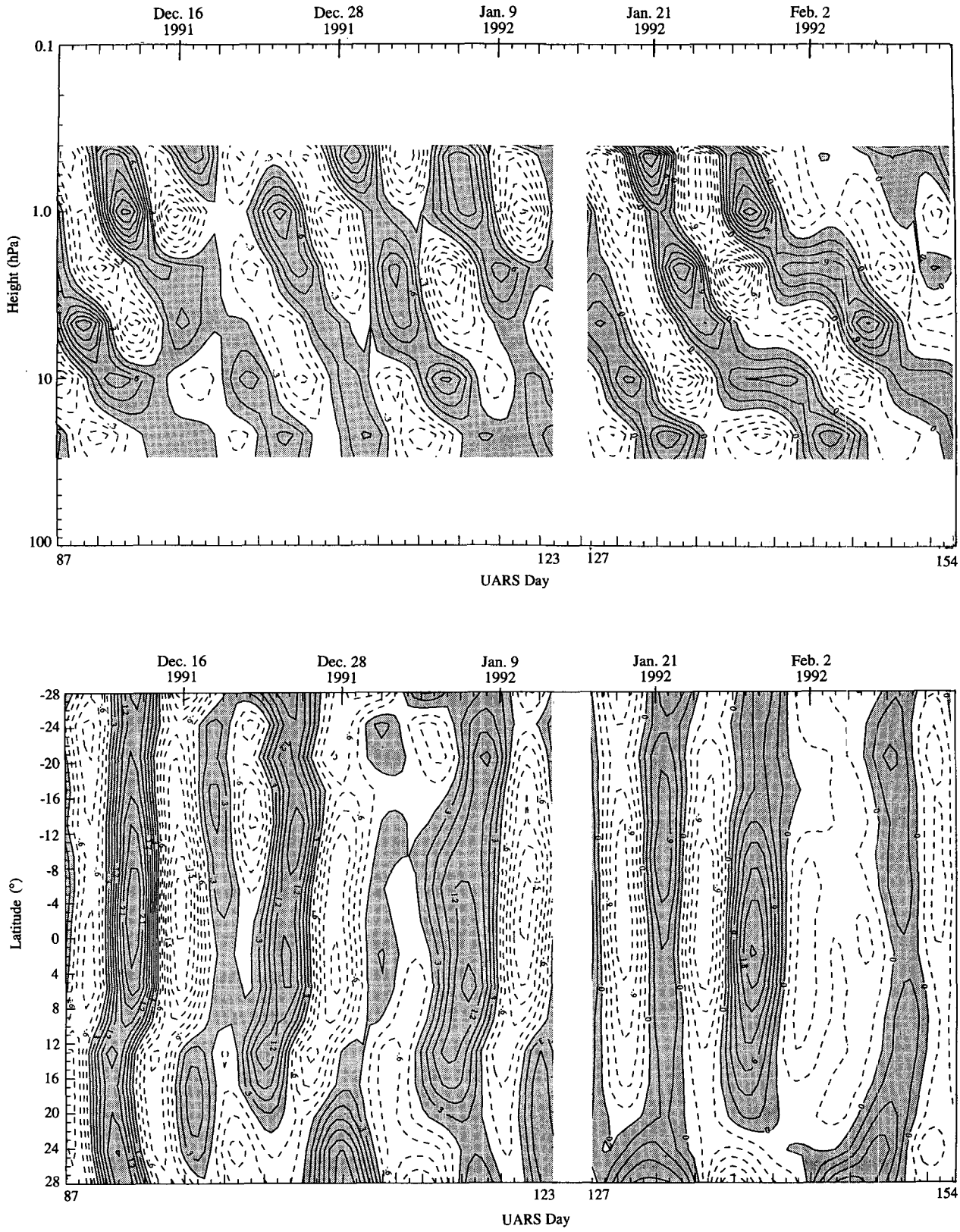

FIG. 3. (a) Time–height plot at the equator and (b) latitude–time plot at 1 hPa of temperature zonal wavenumber 1, bandpassed for periods between 5.5 and 20 days, during period I, at 0° longitude. Positive values are highlighted in gray. (Contour interval is 0.3°C.)

ory). Although there is clearly equatorial trapping, these oscillations are not exactly symmetric about the equator, and furthermore, the latitude of maximum amplitude oscillates throughout the sample. The center of the wave tends to be more often displaced toward the south, that is, toward the summer hemisphere.

The next wave band analyzed includes periods between 5.5 and 3 days. This corresponds to the band where ultrafast Kelvin waves were first reported by Salby et al. (1984). In general, the plots (not shown) are dominated by an oscillation with descending phase and a period slightly shorter than 4 days, again in agreement with the LIMS analysis. The sporadic nature of the wave is more noticeable since the oscillation reaches only a relatively large amplitude in the middle of the sampled period. During the time of maximum amplitude it can actually be observed almost as low as 20 hPa. The vertical wavelength during this stage is of the order of 44 km, the horizontal phase speed is approximately 115 m s^{-1}, and the width at 1 hPa, as defined above, is of the order of 14°, which is substantially less than given by linear theory. The peak to peak range is of the order of 2.4°C. As before, the latitudinal structure is not centered about the equator. The oscillations lose their clearly defined equatorially trapped Kelvin wave character when the amplitude is low.

Analysis of the oscillations in zonal wavenumber 2 was carried out for period bands between 4.5 and 17 days, and 2.3 and 4.5 days, respectively. As before, both cases yield evidence of Kelvin wave activity. Analysis of the lower-frequency spectral band indicates that the period shifts from 5–6 days at the beginning of the sample period to approximately 7 days in the second half of the sample period, with a corresponding reduction in the vertical wavelength, from about 15 to 12 km. The horizontal phase speed in this case is 33–46 m s^{-1}. The latitudinal extent of the oscillation is of the order of 42°, at the time of largest range (peak to peak: 2.4°C), for the faster waves and 24°–30° for the 7-day wave. Again the center of the oscillation seems to be predominantly displaced toward the summer hemisphere. A disturbance was observed to progress upward from the lower region during the first part of the sample. Another, though less well defined, is visible after the break due to the yaw.

The dominant period for the faster wavenumber 2 (Fig. 4) is of the order of 3.5–4.5 days, with a vertical wavelength of 20 km and a horizontal phase speed of 52–66 m s^{-1}. The latitudinal extent of these oscillations is in the vicinity of 22°–26°, with amplitudes as large as 1.8°C. There appear to be a series of discrete upward-propagating amplitude maxima throughout the sample. A close comparison of Figs. 3a and 4a suggests that the amplitude maxima propagating upward in zonal wavenumbers 1 and 2 tend to be simultaneous.

Examples of meridional cross sections for zonal wavenumbers 1 and 2 at longitude 0° are shown in Fig. 5 (see also Table 1). These each show the latitude–height structure of the temperature perturbation for a particular frequency band on a given day. The meridional distributions show a height-dependent shift toward the summer hemisphere, which is more marked as height increases. The overall structures are, however, generally consistent with the equatorial Kelvin wave structure.

As expected from the easterly mean zonal flow during this period, the Kelvin waves are very well defined in the fast and ultrafast wave bands for zonal wavenumber 1 and the fast wave band for zonal wavenumber 2. Furthermore the observed periods, wavelengths, and other parameters are in excellent agreement with the results from LIMS and the theoretical predictions as given in Salby et al. (1984). Another interesting feature in approximate accord with Salby et al. (1984) is the close relationship between the wavenumber 1 disturbance of 8-day period and the wavenumber 2 quasi–4-day wave. As suggested in that paper, given the nondispersive character of zonal Kelvin waves, it is possible that these two particular waves are zonal harmonics of a discrete synoptic perturbation.

Figures 6 and 7 show examples of the behavior of eastward propagating waves during period II. An overview of the plots shows that in most cases the Kelvin wave signatures are not as well defined as during period I. In Fig. 6 there are two possible Kelvin wave events, one near the beginning and one near the end of the sample. In between these there exists a span of time with no well-defined wave signatures, although there appears to be an increase in activity toward the southern limit of the region under study (the subtropics of the winter hemisphere).

Figure 6a clearly shows a change in the slope of phase lines between the middle and upper stratosphere during the first wave event. This corresponds to a reduction in wave period from about 8 to 6 days between 9 and 1 hPa. The vertical wavelength in the upper section of this disturbance is of the order of 20 km, and the peak to peak range of the wave is of the order of 2.8°C. A very rough estimate suggests a wavelength of 12–14 km in the lower-altitude portion of the perturbation. The horizontal phase speed range is 58–77 m s^{-1}. The second wave event appears to have a periodicity of 8–9 days. Again a rough estimate suggests a vertical wavelength of 16–18 km. The latitudinal extent at 1 hPa for the first event is on the order of 28°–32°, shifted toward the summer hemisphere. The second event appears to have a similar latitudinal scale, though is difficult to confirm due to the presence of important antisymmetric components.

The higher-frequency band of wavenumber 1 has a Kelvin wave signature that has a range of approximately 2°C but exists only during the first portion of the time series. The period of this wave event is about 4.5 days, the vertical wavelength is around 30 km, and the horizontal phase speed is about 102 m s^{-1}. The latitudinal separation between quarter-power points at

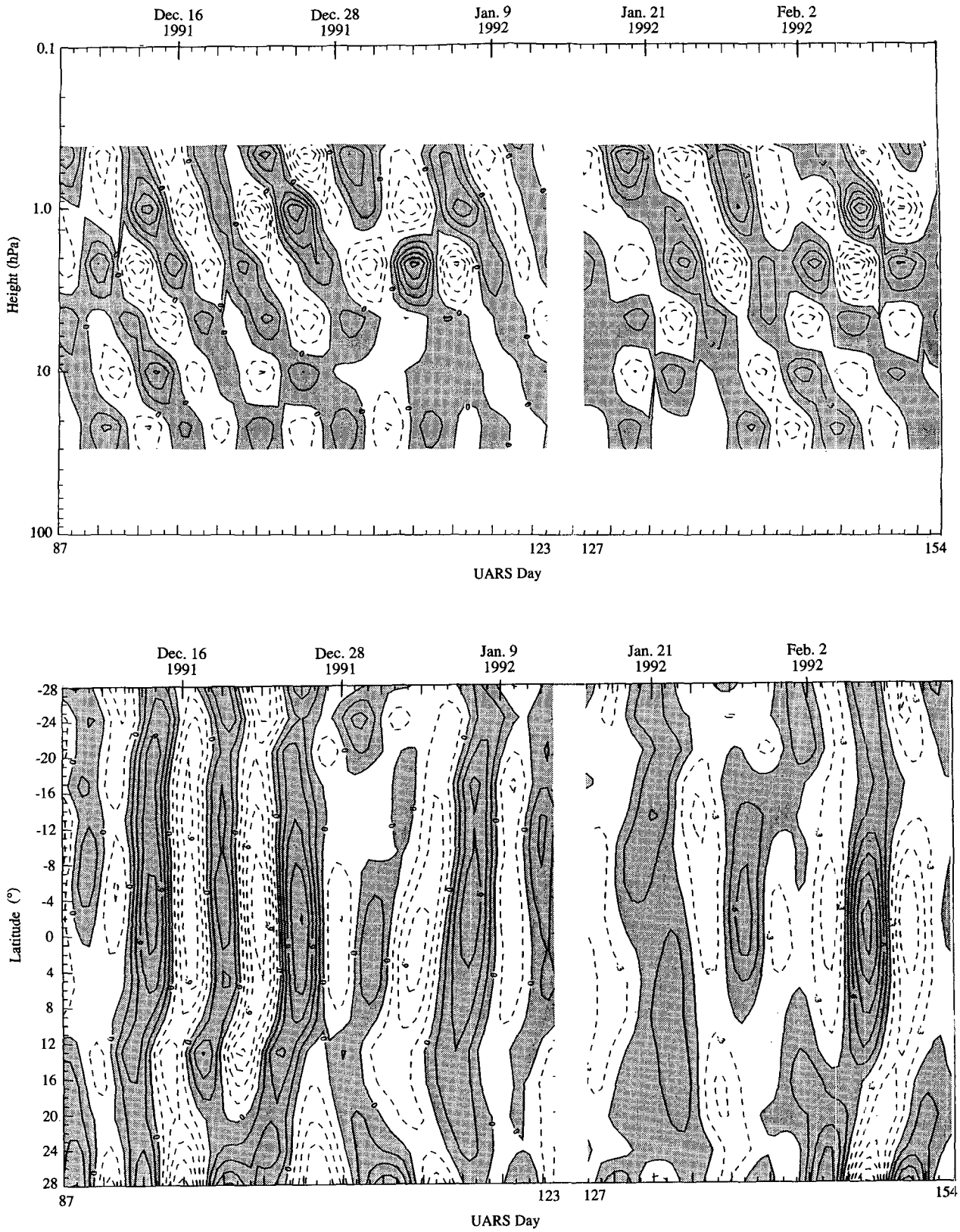

FIG. 4. Same as Fig. 3 but for zonal wavenumber 2 with periods between 2.5 and 4.5 days.

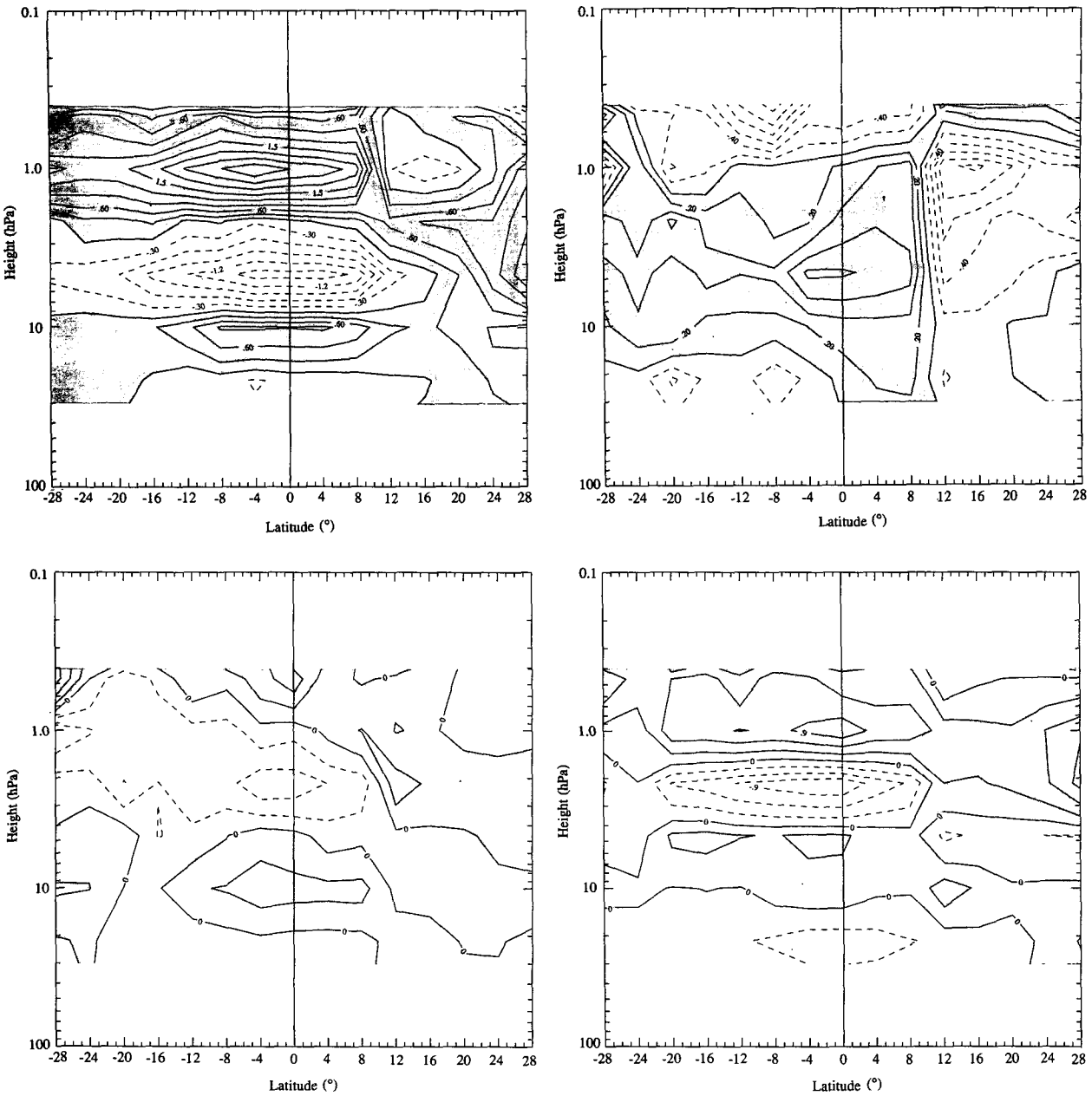

FIG. 5. Examples of meridional cross sections of the waves, during wave events of period 1. These correspond to zonal wavenumber 1 with periods between (a) 5.5 and 20 days and (b) 3 and 5.5 days, and to zonal wavenumber 2 with periods between (c) 4.5 and 17 days and (d) 2.5 and 4.5 days. (Contour interval is 0.3°C.)

1 hPa and during the largest amplitude reached is 24°–28°, which again is somewhat narrower than suggested by linear theory. After the yaw maneuver there is little evidence of systematic downward phase propagation.

Wavenumber 2 was analyzed using period bands of 5.5–17 days and 2.3–5.5 days, respectively. The first band does not seem to contain much evidence of Kelvin wave activity. There is a possible event, during the first 20 days, with an approximate period of 8 days, 1.6°C peak to peak amplitude, and a vertical wavelength of 12–15 km. These values, given the characteristic of the sample, are not very conclusive. The second band shown in Fig. 7, on the other hand, does have a clear Kelvin wave signature representing the fast waves. The period is approximately 4 days for the two events that can be clearly seen in each section of the plots. The vertical wavelength is 20 km, and the horizontal phase speed is near 58 m s^{-1}. The latitudinal range is now

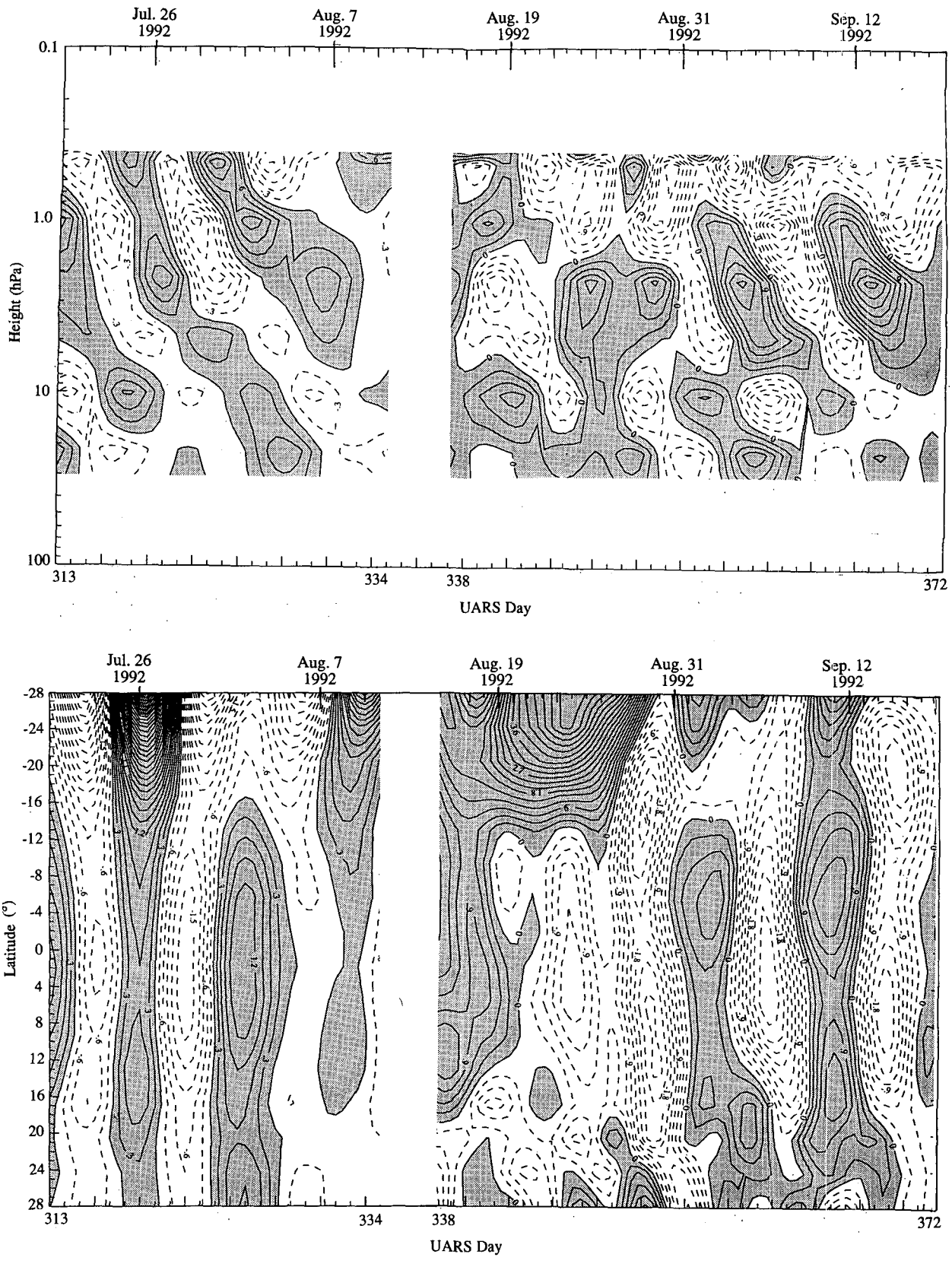

FIG. 6. Same as Fig. 3 but for period II. (Contour interval is 0.3°C.)

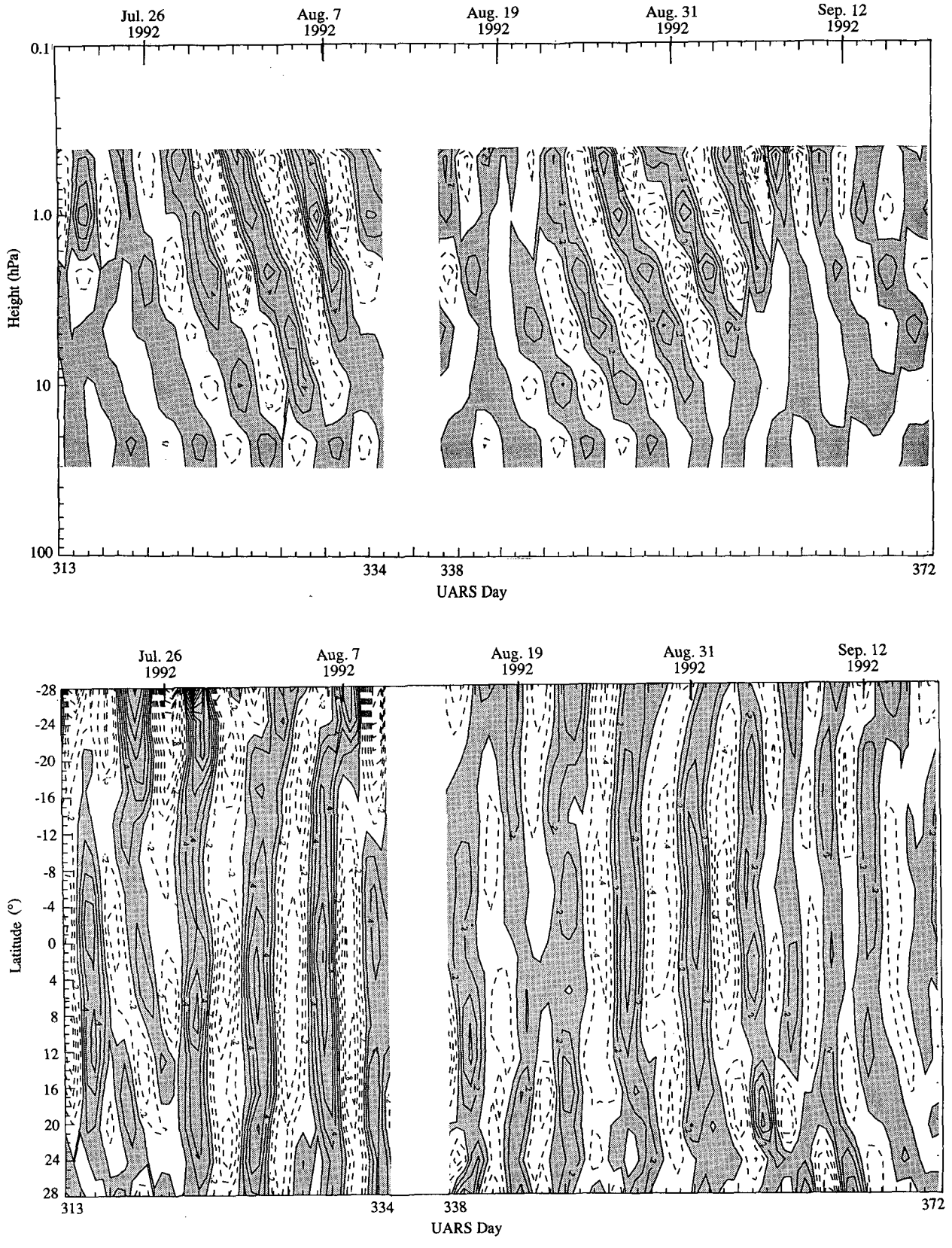

FIG. 7. Same as Fig. 3 but for zonal wavenumber 2 with periods between 2.3 and 5.5 days. (Contour interval is 0.2°C.)

about 38°–42°, which agrees well with linear Kelvin wave theory. As was the case during period I, this particular wave band seems to be linked to the zonal wavenumber 1 fast wave band. The near simultaneity of the wave events and the coincidence of most wave characteristics between this case and that presented in Fig. 6 is striking.

The Kelvin wave nature of these wave bands was further confirmed by plotting meridional cross sections (not shown) for times corresponding to the wave events. These showed again the classical layered structure of a Kelvin wave. The wavenumber 1 components were fairly symmetric about the equator but the wavenumber 2 components were displaced toward the summer (Northern) hemisphere.

At least two factors may be important in accounting for the large differences in Kelvin wave activity between period I and period II. First, the large-scale patterns of tropical convection that are thought to be the major tropospheric sources for Kelvin waves are stronger during the Northern Hemisphere winter (period I) than during Northern Hemisphere summer (period II). Second, as shown in Fig. 1, the mean zonal wind conditions are rather different during the two periods. Period 1 is characterized by a broad region of easterlies in the equatorial region; period 2 has weak equatorial westerlies near 10 hPa, with westerly shear below and easterly shear above. Thus, the Doppler-shifted phase speed of the Kelvin waves will be smaller during period II, and the waves will be subject to larger dissipation. The mean westerlies are too weak, however, to account for much dissipation of the fast and ultrafast Kelvin waves. Nevertheless, the ultrafast zonal wavenumber 1 practically disappears after the yaw maneuver in period II. Furthermore, some of the other Kelvin waves reappear in the middle of period II, though the equatorial westerly mean flow is actually stronger by then. Thus, the lack of a strong wave signature in period II is probably more related to variations in the wave sources than damping due to reduced intrinsic phase speeds.

This hypothesis is supported by the fact that the slower wavenumber 2 and the ultrafast wavenumber 1 are both almost totally absent in the second half of the sample. LIMS results and those from period I for the fast Kelvin waves show that wavenumbers 1 and 2 can be harmonics of a discrete disturbance. In the case of the wavenumber 2, the slower wave would then be the harmonic of a Wallace–Kousky wave. Salby et al. (1984) proposed that the wavenumber 2 harmonic of the slow Kelvin wave can be identified well into the middle atmosphere, while the wavenumber 1 harmonic is not, either because the wavenumber 2 is selectively enhanced by the driving mechanism or because it has twice the intrinsic frequency and thus experiences less absorption.

The prevailing conditions in period II allow for absorption of the slow wavenumber 1 component below 10–20 hPa (although the westerly flow remains too weak to create a critical layer for a 15–20-day wave). However, the higher-frequency wavenumber 2 harmonic and the fast wavenumber 1 mode should not experience much absorption. Because these frequency bands appear to weaken in the second part of period II, it is likely that the Kelvin wave driving mechanism is weaker or has at least changed its spectral composition. It must be remembered that this sample actually lasts well into September (i.e., near the equinox), by which time the Kelvin wave season is usually coming to an end (Randel and Gille 1991).

4. Spectral analysis of the temperature and ozone fields

The above time series analysis demonstrates that MLS measurements yield strong evidence supporting the presence of Kelvin wave activity in zonal wavenumbers 1 and 2 during the first two solstices of the *UARS* mission. In this section the frequency spectra of these wavenumbers are examined for the temperature and ozone fields. The "raw" spectra obtained as an intermediate product of the asynoptic mapping method are shown. Only the spectra corresponding to the longer observational sequences are presented—that is, those that were obtained from more than 32 days of continuous measurements. This allows for an acceptable degree of resolution and statistical stability. The spectra shown were further smoothed by a latitudinal running average, three latitudes at a time. The lower frequencies have been blocked out in the diagrams for the sake of clarity.

The power spectra for temperature in zonal wavenumbers 1 and 2 during the first 39 days of period I can be seen in Fig. 8. These spectra are in very good agreement with the reconstructed time plots, with distinctly defined bands. In Fig. 8a the fast wave, with a period of 7.5 days (shifting to 6.5 days near and above the stratopause), and the ultrafast one, with a periodicity of 3.8 days in the upper stratosphere, can be observed. There also appears to be some power in the region corresponding to the Wallace–Kousky wave, with a period between 12.5 and 20 days. Given the easterly flow that would increase the intrinsic frequency of the wave and the observed characteristic shift toward higher frequencies as height increases, the existence of such a wave is plausible. On the other hand, radiative damping has a timescale that is of the same order (approximately 10 days) as the period of the wave in the upper stratosphere, and in consequence, the wave should be damped with height. However, it must be remembered that this spectral band includes only a very limited number of realizations in its determination, due to the short length of the time series, and thus must not be overinterpreted. Finally, the westward variance near 12 days observed above the stratopause appears to be linked to wave activity that penetrates

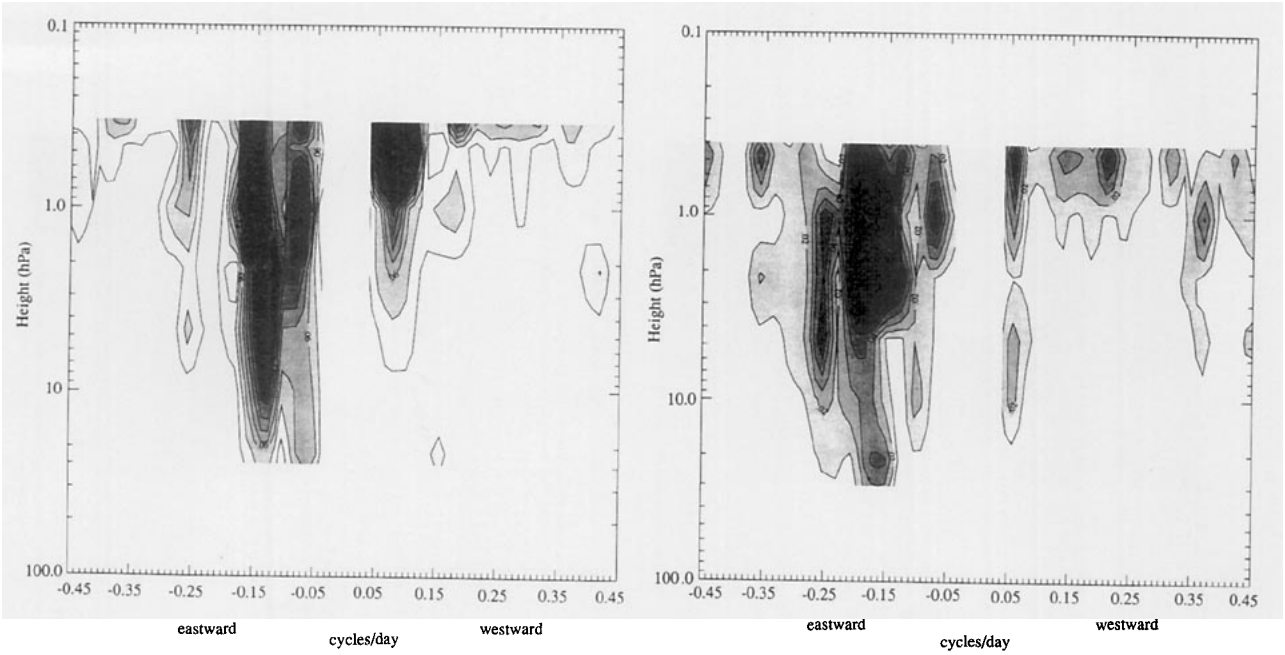

FIG. 8. (a) Zonal wavenumber 1 and (b) wavenumber 2 power spectra during the first 39 days of period I, averaged in latitude about the equator. [Contour interval is (a) 0.025 K^2 and (b) 0.01 K^2.]

from outside the equatorial region, as observed in latitude–frequency plots. The plots show enhanced westward spectral power penetrating from the edge of the sampled region.

The spectrum of zonal wavenumber 2, as seen in Fig. 8b, has two strong bands—one with a dominant periodicity near 5.7 days, and a weaker one at 3.8 days—in agreement with the analysis in the previous section. Furthermore there is a tenuous signal at periods between 2.6 and 3 days. The slower mode is strongest near the stratopause, though it is present throughout the height range of the sample and shows the characteristic shift to higher frequencies with height. As in the previous case there is evidence of westward wave activity in the lower mesosphere.

By integrating frequency over narrow bands corresponding to the spectral signatures in Fig. 8 it is possible to obtain information on the meridional cross sections of the Kelvin waves in the various frequency bands. The latitude–height amplitude structure of the fast Kelvin wavenumber 1, integrated between 5.6 and 9 days, is shown in Fig. 9a, and the same wave decomposed into symmetric and antisymmetric components about the equator is shown in Fig. 9b. The decomposition shows that most of the observed variance is due to the symmetric component as expected for a Kelvin wave. The displacement toward the summer hemisphere observed in the latitude–time plots at 1 hPa can also be seen through most of the height range. Below about 2 hPa, the latitudinal width is limited, but above that height there is a rapid increase. It must be remembered that the zonal flow (Fig. 1) for this period shows a westerly vertical shear near 5 hPa, and this can cause a constriction of the wave. However, as shown in Table 1, the Doppler shifting of the period in the simple linear theory is not sufficient to account for the observed constriction since the meridional scale varies only with the square root of the intrinsic frequency. Above the 2-hPa level there is a return to a weak easterly vertical shear, coincident with the rapid broadening. Most of the asymmetry is located at the edge of the equatorial region. The meridional cross section for the ultrafast mode was obtained for periods between 3.6 and 4.6 days (Figs. 9c and 9d). The broader latitudinal structure of this mode is in agreement with LIMS results and the analysis in section 3. The fact that it does not reach a considerable amplitude until near the stratopause is evident again. Also, as with the fast wave, the antisymmetric component is limited to the high latitudes of the region under consideration.

The latitude–height distribution of wavenumber 2 temperature amplitude integrated over the period range 4.6–7.2 days is shown in Fig. 10. As with the fast wavenumber 1, the latitudinal scale is limited below 2 hPa and grows rapidly above that level. The maximum amplitude is reached near 1 hPa, as was true for the LIMS data for a similar wave. Another interesting feature is that the antisymmetric component is far weaker than for wavenumber 1.

The spectral behavior of the ozone mixing ratio field is shown in Fig. 11. Spectral power is concentrated in the regions of strong vertical gradients of mixing ratio, that is, below and above the ozone layer maximum, which MLS measurements place near 10 hPa, during

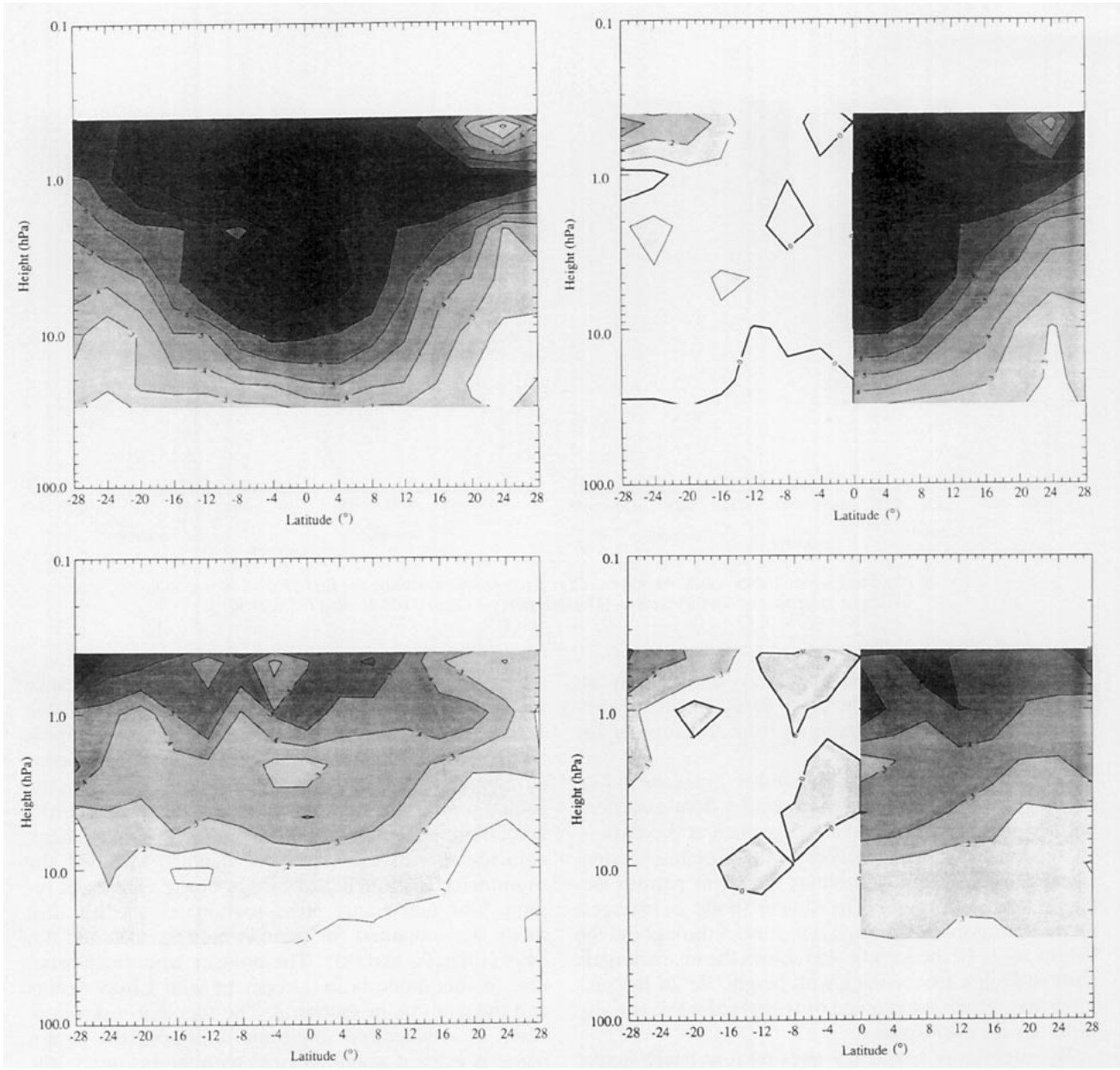

FIG. 9. Meridional cross sections of temperature amplitude for zonal wavenumber 1, integrated between 5.6 and 9 days [(a), (b)] and 3.6–4.6 days [(c), (d)] during period I. Plots (a) and (c) show the amplitude resulting from the integration. Plots (b) and (d) show the decomposition of the cross sections into symmetric (right side) and antisymmetric (left side) components. (Contour interval is 0.1°C.)

this sample. This is in agreement with the perturbation equation (1) since below 10 hPa it is the vertical advection by the Kelvin wave that generates the ozone perturbations, while above 10 hPa it is primarily the temperature dependence of the ozone photochemistry that generates the Kelvin wave–related signal in ozone.

At frequencies corresponding to the slow Kelvin wave, a relatively large perturbation can be observed. As in the case of temperature, this is not easily interpreted from the short time series given its low frequency. It must be noted however that this feature, and its increase in frequency with height, is coincident with the signature in the temperature spectrum (Fig. 9a). The two remaining eastward features, above and below the mixing ratio peak, agree in frequency with the spectral analysis of the temperature. In the westward frequency range there is a strong signature near the 10-hPa level where the mean field has its maximum. This has also been reported in LIMS data (Salby et al. 1990) and is visible in Fig. 3 of Randel (1990). According to Salby et al. (1990) this signature could be caused by large planetary waves, which may propagate

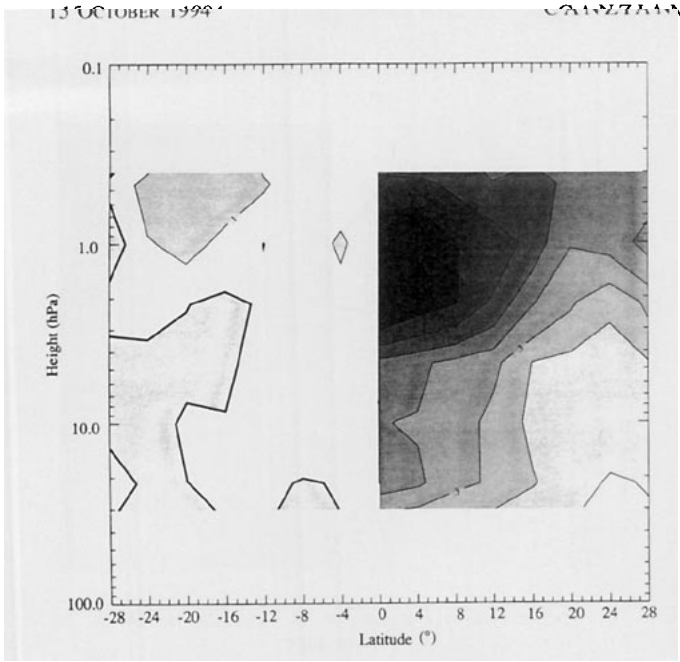

FIG. 10. Meridional cross section of amplitude for temperature, zonal wavenumber 2, integrated between 4.6 and 7.2 days during period I.

through the easterlies into the stratospheric equatorial region. Such disturbances tend to have a nearly barotropic structure, with very weak temperature perturbations. Nevertheless, they may induce changes in the mixing ratio through meridional advection.

The spectra shown here do differ from the results of Randel (1990) and Salby et al. (1990) in that the dependence on the vertical gradient of mixing ratio is far more evident. LIMS Version 4 data used in both of these LIMS analyses does not show evidence of wave activity near the 6-day period below 10 hPa. LIMS Version 5 data, also included in Randel (1990), show somewhat more power in this region, particularly for frequency band–integrated meridional cross sections. It must be noted that according to Sun and Leovy (1990), LIMS Version 5 data for ozone are better than the Version 4 data.

The dominant eastward signal for wavenumber 2 (Fig. 11b) again shows minima in spectral power near the 10-hPa altitude of maximum ozone mixing ratio. This signal corresponds to the first harmonic of the slow, zonal wavenumber 1 Kelvin wave and has a period near 6.5 days in the lower region and near 5 days close to the stratopause. As was the case of the temperature wavenumber 2, a weak signal can be seen near the 2.6–3-day period band. The strongest westward signature again appears at low frequencies near the altitude of maximum mixing ratio. There is some power scattered at other westward frequencies. The comparison with LIMS Version 4 and Version 5 data in this case is not very good. The Version 4 data show maximum power close to or above the maximum ozone, while V5 yields significant power only below 10 hPa (Randel 1990).

Latitude–height plots for the perturbation ozone amplitude in the same frequency bands as shown for temperature in Fig. 9 are displayed in Fig. 12. For the fast Kelvin waves (Fig. 12a) two distinct regions can be seen above and below the ozone maximum. The struc-

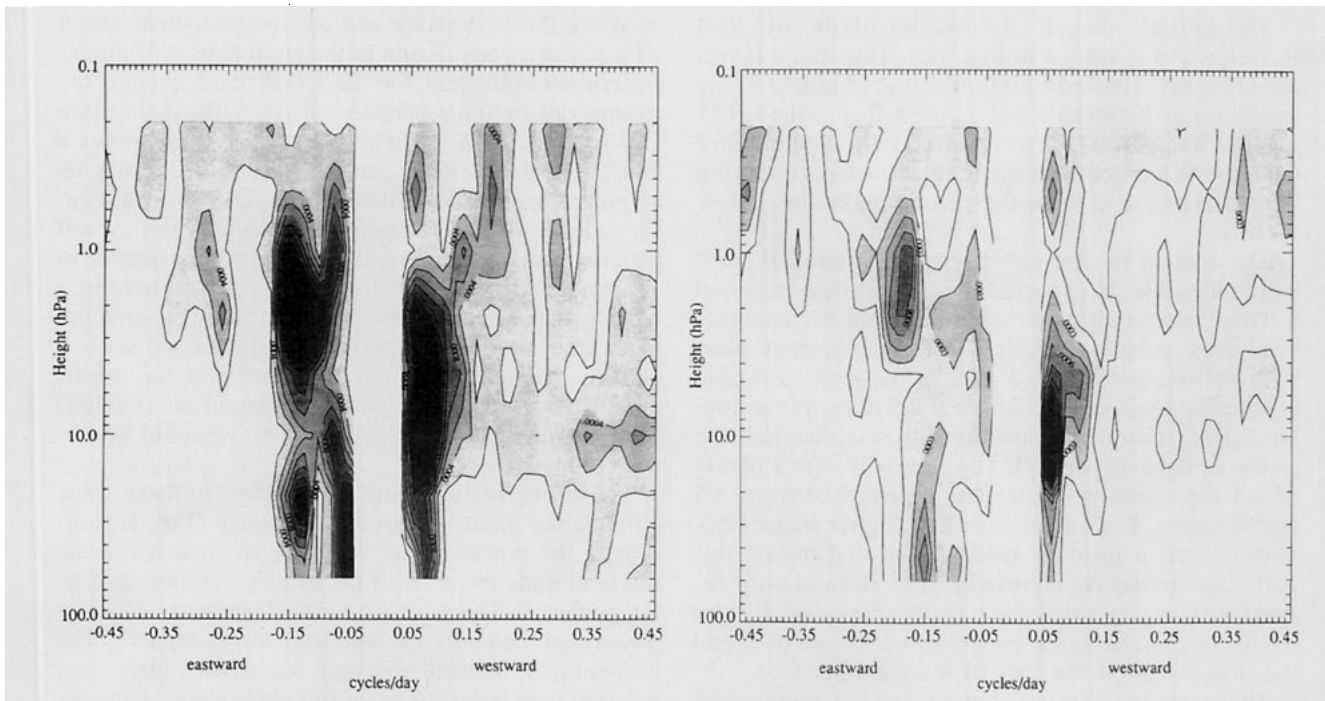

FIG. 11. Same as Fig. 8 but for the ozone mixing ratio during period I. [Contour interval is (a) 0.0002 ppmv² and (b) 0.0001 ppmv².]

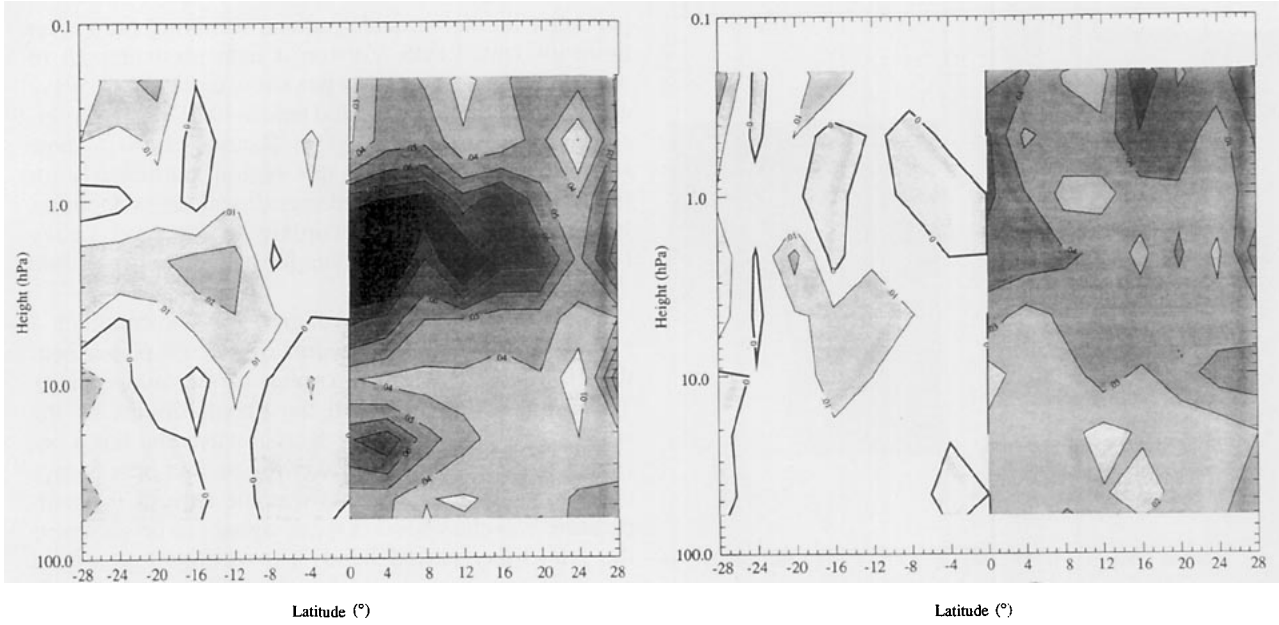

FIG. 12. Same as Fig. 10 but for ozone mixing ratio amplitude, zonal wavenumber 1. Plot (a) corresponds to periods between 5.6 and 9 days, and plot (b) to periods between 3.6 and 4.6 days. (Contour interval is 0.01 ppmv.)

ture above 10 hPa is strikingly similar to that in the LIMS observations (Fig. 7, Salby et al. 1990), though the asymmetric component is not as strong in this case, and the maximum above 10 hPa reaches its peak amplitude at a greater height than in the LIMS observations. The secondary maximum below the 10-hPa level is far stronger in the MLS data than in the LIMS Version 4 data analysis.

The latitude–height distribution of the ultrafast Kelvin wave is shown in Fig. 12b. The signal is relatively weak, limited in latitude, and confined to the height range between 3 and 0.2 hPa, just as the LIMS results. The results corresponding to wavenumber 2 (not shown) agree with the temperature perturbation (Fig. 10) and also show the second maximum below 10 hPa.

The spectra for the last 36 days of period II yield amplitudes that, as expected, are smaller than in period I. The temperature perturbation in zonal wavenumber 1 appears to be essentially a narrow frequency band with periods between 8.5 and 12 days; there is also apparently a weaker oscillation at 6.5 days. Wavenumber 2 has spectral components with less than half the power of those in period I. The slow wave has a period of 6.5 days, and the faster one a period between 3.5 and 4.5 days. Both show a shift to higher frequencies with height. It must be remembered that during this particular period the composite plots showed only defined Kelvin wave structures for the faster of the two bands that appear in the spectra in wavenumber 2, and the slower band in the case of wavenumber 1.

The meridional cross sections for the main zonal wavenumber 1, integrated between 7.7 and 14.6 days, has a weaker amplitude than the fast Kelvin wave during period I. It maximizes in the vicinity of the stratopause but is narrower at that height. The asymmetric component is present as usual at the higher latitudes, though this time its relative amplitude is larger than during period I. A similar analysis for the wavenumber 2 cross section, at periods between 3.3 and 4.6 days, yielded a pattern with appreciable amplitudes only near or above the stratopause and narrow latitudinal extent with a major constriction at the stratopause. A similar pattern was obtained for the LIMS data, though the strong constriction was observed at 0.5 hPa in that case (Salby et al. 1984). Though the zonal wind shows a trend toward a westerly vertical shear above 1 hPa, its magnitude cannot be sufficient to explain this behavior. The antisymmetric component shows that the overall pattern is shifted toward the summer hemisphere, in agreement with the meridional cross section during a wave event. It must be noted that the slower signature when integrated over a narrow band does not show a defined structure. This is coincident with the results obtained with the wide band mapping in the previous section, where no distinct Kelvin wave could be observed.

The ozone perturbations in response to these weak temperature perturbations are also weak (Fig. 13), although the power in the very low frequencies in the lower-altitude region is of the same magnitude as during period I. The westward signal appears with less power and then only for the zonal wavenumber 1. The best defined eastward signature for wavenumber 2 has a period near 4 days. The eastward frequency band for ozone wavenumber 1 coincides with that for tempera-

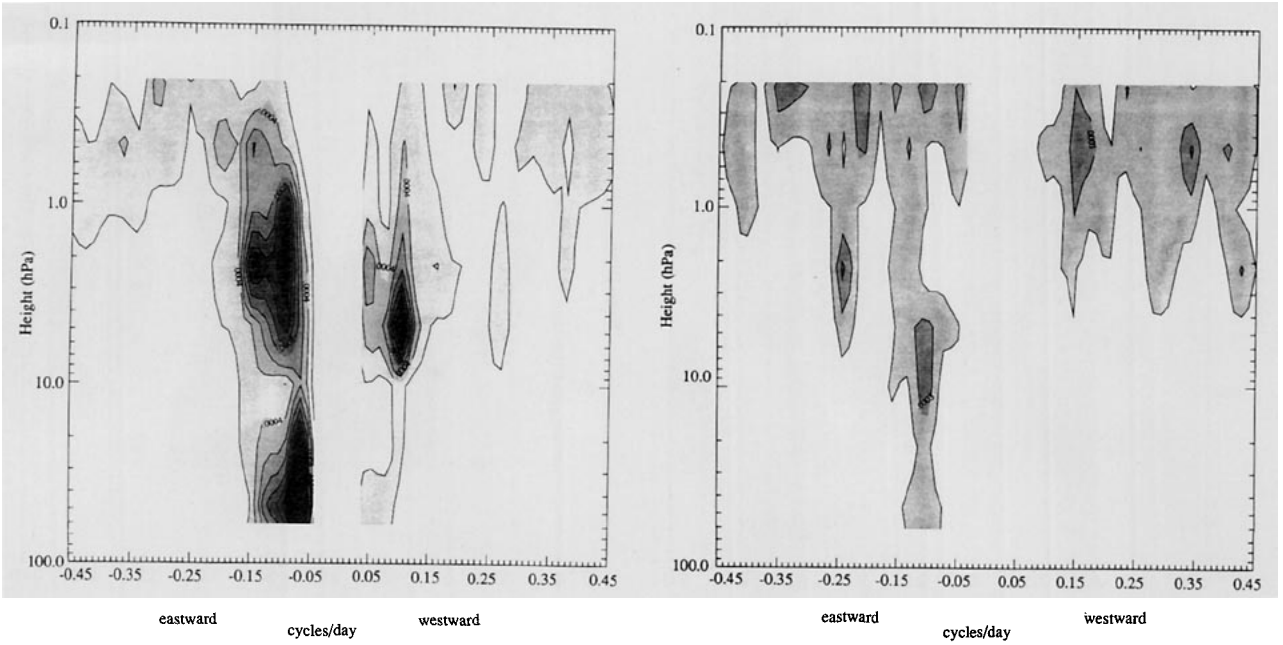

FIG. 13. Same as Fig. 8 but for the ozone mixing ratio during the last 36 days of period II.

ture in wavenumber 1 (Fig. 11a), but the agreement is less good for wavenumber 2.

The latitudinal cross section of ozone (not shown), plotted for the same frequency band as the wavenumber 1 temperature perturbation, has a structure that, except for the minimum near 10 hPa, is close to that of the temperature. There is some activity near high-latitude edges of the region, and the antisymmetric component yields a displacement of the overall pattern toward the summer hemisphere. Though not shown, the 3.3–4.6-day ozone perturbation is in good agreement with the similar wave during period I, albeit with a reduced amplitude.

This overview of the "raw" spectra shows that the wide band mapping is an effective approach to the study of the Kelvin waves, when the time series available are relatively short, and that some features in the spectra that might appear at first as a Kelvin wave signature must be carefully analyzed. This is the case, for example, for the apparent slow wavenumber 2 mode during period II.

The close relationship between the temperature and ozone perturbation can also be seen in this analysis. The spectra for the two fields have many common features, particularly in the eastward-propagating modes. This relationship is reviewed in more detail in the next section.

5. The relationship between temperature and ozone

A more detailed study of the relationship between the temperature and ozone perturbations was carried out following the procedure mentioned in section 2. Two spectra in each period were averaged for each atmospheric variable. The coherency squared, which shall be referred to as coherency for the sake of simplicity, was then evaluated following Randel (1990). In Fig. 14, examples of the coherency during period I are shown. In both cases the highest level of coherency is reached for frequency bands that have important signatures in the averaged spectra. The coherency plots shown in Randel (1990) do not show such a band-dependent structure, probably because of the differences in determination of the spectra and the greater length of the sample in that paper. However, despite these differences the agreement is good for wavenumber 1. Note that there is a certain degree of coherency for wavenumber 1 in the westward direction, particularly in the lower frequencies. The meridional cross section for a band centered at 10 days (eastward) for zonal wavenumber 1 yielded patterns similar to those obtained with LIMS V4 data. The one corresponding to a 5-day band (eastward) for zonal wavenumber 2 is shown in Fig. 14c. Notice that for the 99% confidence level the pattern is separated into two distinct lobes above and below the mixing ratio maximum.

Figure 15 shows the result of a similar coherency analysis for period II. The general pattern again shows high levels of coherency for eastward-moving waves in the frequency and height range of the waves detected in the previous sections. As was the case of period I, a high degree of coherency can also be observed for the slowest westward frequencies. On the other hand, the meridional cross section for the 6-day band (Fig. 15b) shows such a coherency structure, with high confidence

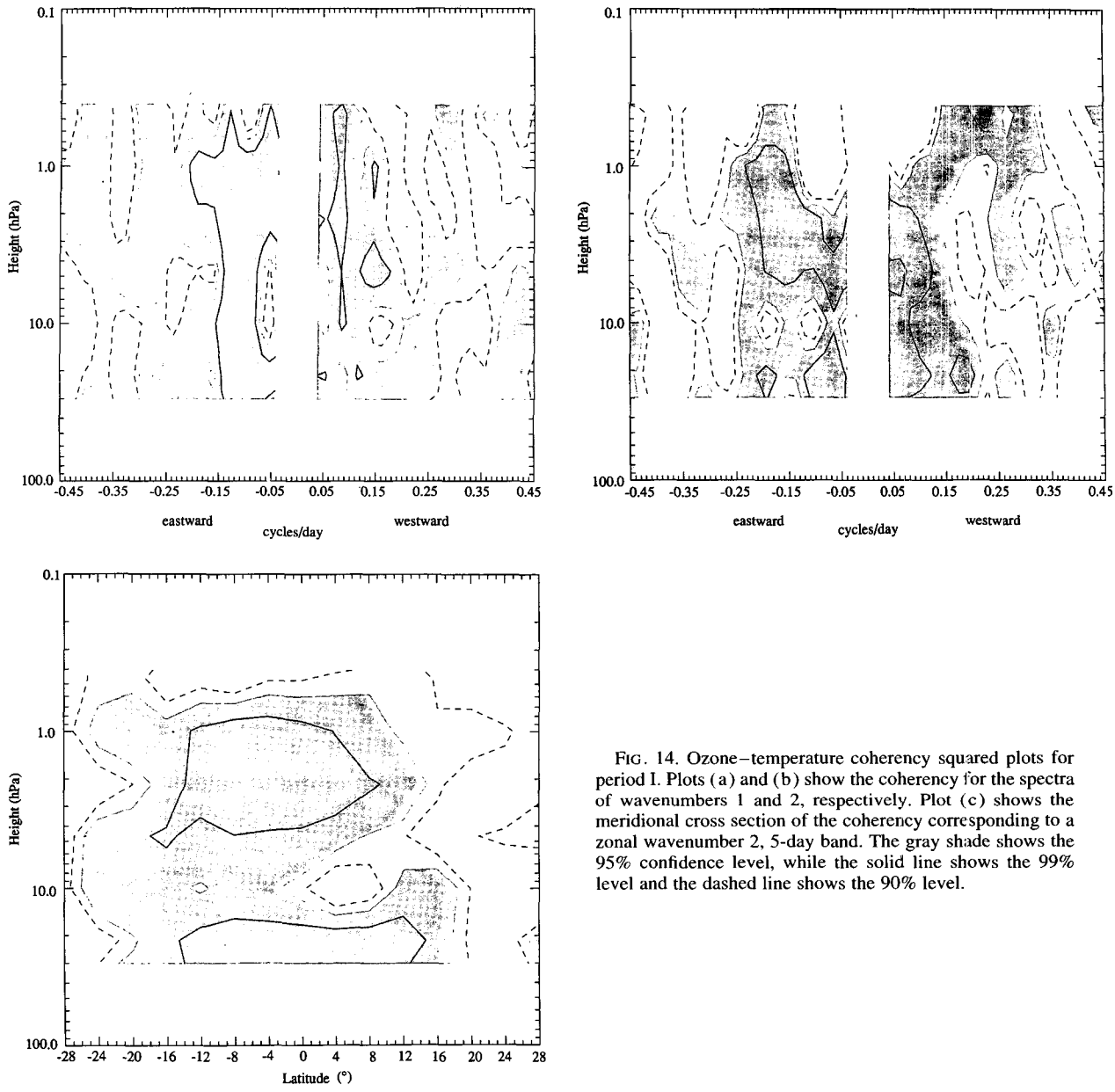

FIG. 14. Ozone–temperature coherency squared plots for period I. Plots (a) and (b) show the coherency for the spectra of wavenumbers 1 and 2, respectively. Plot (c) shows the meridional cross section of the coherency corresponding to a zonal wavenumber 2, 5-day band. The gray shade shows the 95% confidence level, while the solid line shows the 99% level and the dashed line shows the 90% level.

levels basically above the 10-hPa surface, agreeing well with previous observations in Randel (1990).

The coherency found for zonal wavenumber 2 (Fig. 15c) differs from that found during period I. There is a high level of confidence for westward-propagating oscillations in the region of high mixing ratio not observed during period I. For eastward propagation, the plot shows that a high degree of coherency is reached only in the upper stratosphere and confirms the conclusion that the faster Kelvin wave structure (period close to 4 days) was the dominant mode for this zonal wave throughout the region under study. The meridional cross section for the 4-day eastward period band (Fig. 15d) also shows a structure that is in agreement with results for other frequency bands.

The LIMS results of Randel (1990) show a defined break in the coherency between the upper stratosphere (above 10 hPa) and the region below 20 hPa, even though the power spectra for both versions of the data did not show evidence of such a feature. Considering the change from ozone perturbations caused by transport below 10 hPa to a regime dominated by photochemistry above 10 hPa, it is reasonable to expect an intermediate region with a low degree of coherency. For example, LIMS Version 4 data coherency (Fig. 5, Randel 1990) shows high confidence levels at 20 and

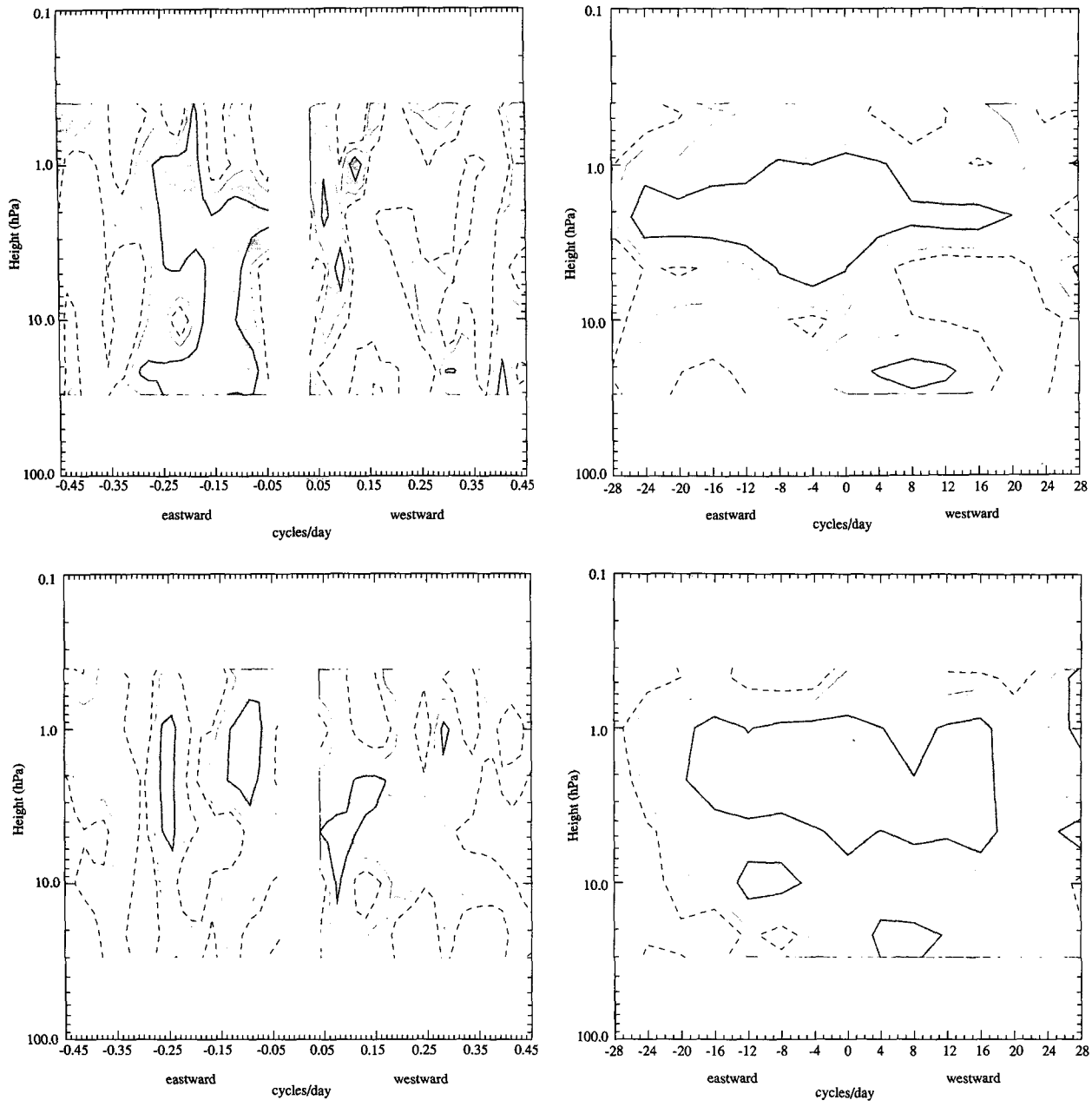

FIG. 15. Same as Fig. 14 but for period II. Plots (a) and (c) show the coherency for the zonal wavenumbers 1 and 2, respectively. Plot (b) presents the meridional cross section of the coherency for zonal wavenumber 1, 6-day band, while plot (d) presents the cross section corresponding to the 4-day band.

10 hPa, with a break in between. The MLS data, on the other hand, generally showed a much smaller reduction in coherency near the 10-hPa surface. A possible explanation for this difference is that the pressure surfaces in the current MLS retrievals have about two-times-coarser vertical resolution of those in the LIMS retrievals. This different resolution becomes more obvious at this stage because the coherency analysis can show high degrees of coherency even for weak signals, as long as the variables are related. When these are plotted without the appropriate degree of resolution, the results may differ.

Finally, Figs. 16 and 17 present the amplitude ratio μ'/T' and the phase lag of the ozone perturbation with respect to the temperature perturbation. The transition from an in-phase-transport-dominated fluctuation to an out-of-phase photochemical regime is clear in all plots. The agreement of this phase lag with that obtained by

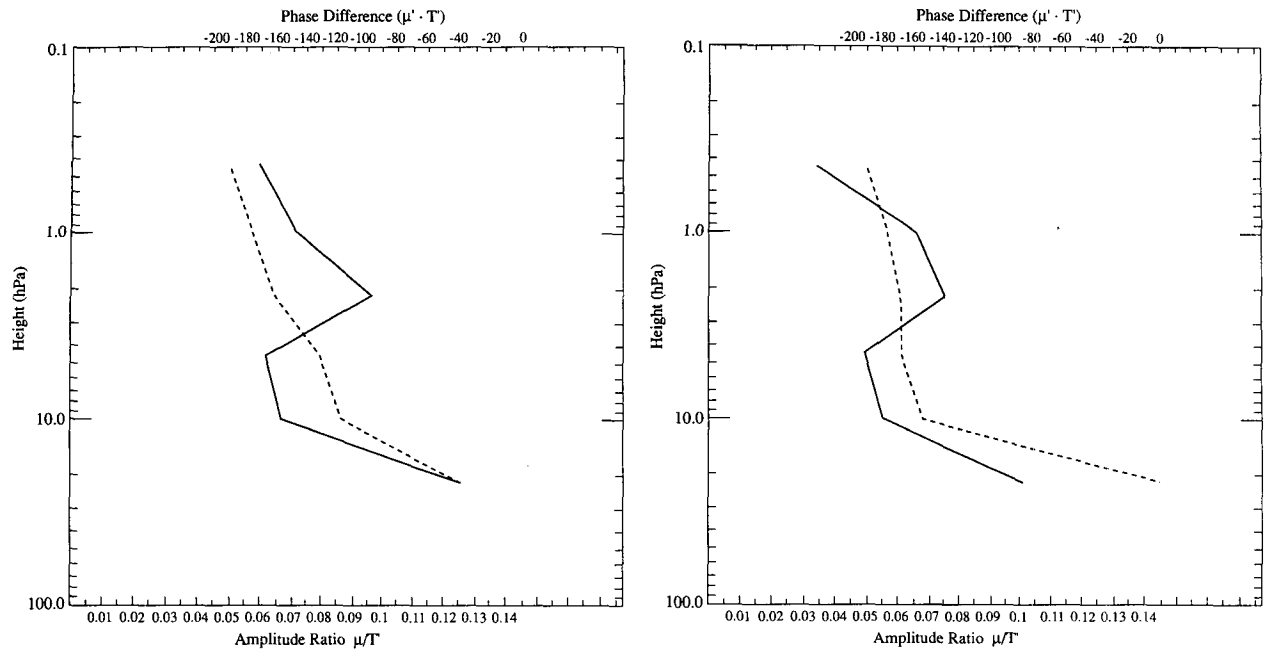

FIG. 16. Ozone–temperature amplitude (solid line) and phase difference (dashed line) for period I. Plot (a) shows the results for zonal wavenumber 1, 9-day band, and (b) zonal wavenumber 2, 5-day band.

the model presented in Randel (1990) is good, and with respect to the LIMS data, period I resembles more the result of Version 5 data. The phase plot for the wavenumber 1 sample of period II is not in as close agreement with theoretical expectations; at upper levels it shows a phase difference greater than 180°, which continues to increase with height. On the other hand, the wavenumber 2 sample, which was much better resolved in the height–time plots, has the expected phase behavior.

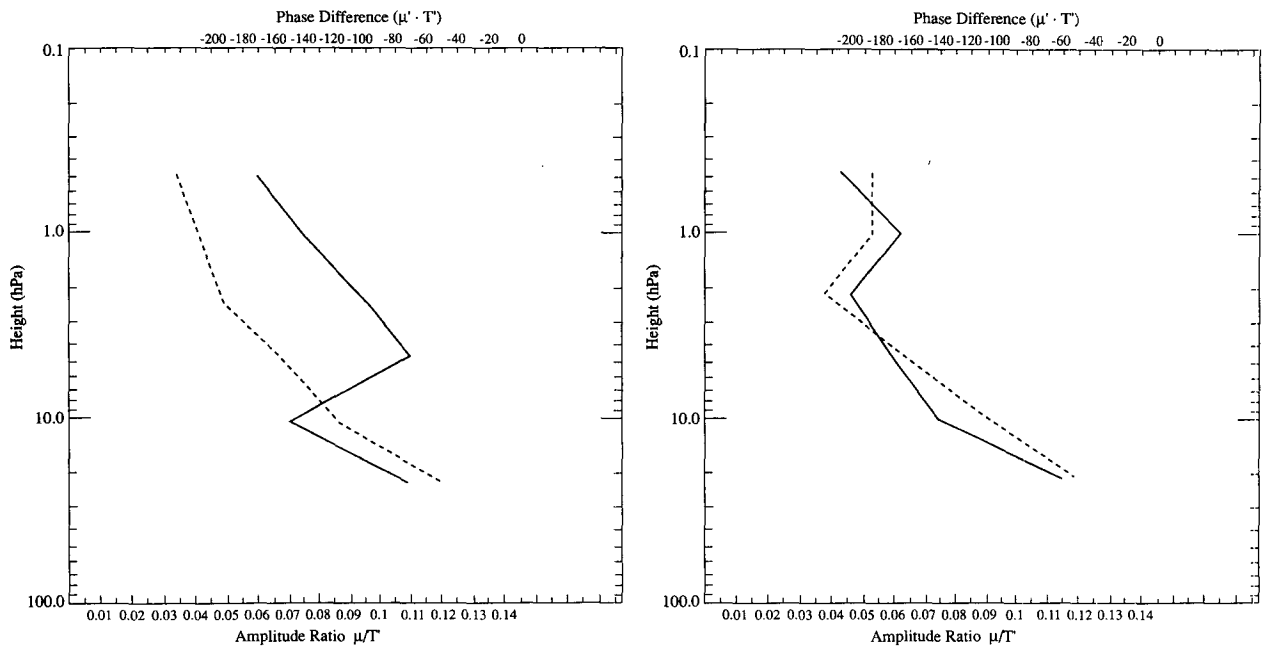

FIG. 17. Same as Fig. 16 but for period II. This time the plots correspond to (a) 6-day band zonal wavenumber 1, and (b) 4-day zonal wavenumber 2.

In all cases the amplitude ratio above approximately 5 hPa was systematically larger than expected from the linear model and from LIMS. Model estimates, as given in Randel (1990), give an amplitude ratio at 1 hPa that, for the Kelvin modes considered here, is dominated by the ratio Θ/Γ. [See Eq. (3a) in Randel (1990).] The quotients obtained here above 5 hPa are larger than those deduced by Randel (1990) from the LIMS data by as much as 60%–90%. At 10 hPa, the quotients are somewhat larger than predicted, particularly in the case of the zonal wavenumber 2 example during period II. However, the amplitude ratios near 20 hPa do agree with the model estimates. In this particular case, a minimum in the amplitude ratio does not occur near 10 hPa but rather near 2 hPa. A comparison of the LIMS amplitudes for temperature and ozone with the MLS results does show that during period I the temperature amplitudes in equivalent frequency bands are smaller for MLS than for LIMS in the upper stratosphere. This may reflect the different periods sampled by the two instruments. The ozone maxima, as has been said before, appear at higher levels in MLS retrievals than in LIMS, and thus, the ratio in this region is increased.

It thus appears that while the correct phase behavior is predicted by the linear theory (1), MLS-retrieved Kelvin wave amplitudes do not agree well with the simple linear model in the vicinity of the stratopause. On the other hand, an agreement is obtained in the lower regions. This is the opposite of what was observed in the LIMS experiment.

6. Discussion and conclusions

The present study has demonstrated the existence of Kelvin waves in the MLS measurements. For the first time it has been possible to compare two subsequent periods of Kelvin wave activity during different stages of the QBO, with a limb viewing satellite instrument. Despite the vertical resolution limitations of the currently available MLS retrievals, the results obtained are mostly in agreement with the LIMS dataset, whose measurement were carried out using a different observational technique. Problems in the analysis of the MLS data, due to gaps in the time series caused by the yaw maneuvers, which are necessary for the *UARS* mission, were effectively overcome with the use of the asynoptic mapping technique, which allowed for the reconstruction of synoptic maps. With the information contained in these maps it was possible to look for Kelvin waves using the wide bandpass filter approach to isolate the frequency bands where Kelvin waves have been identified in previous studies. The fact that spectra are obtained as an intermediate step of the method simplifies the analysis procedures. These "wide band" time series allowed for a case study approach based on time–height and time–latitude plots, where Kelvin wave characteristics were first identified in the temperature fields. The episodic nature of the Kelvin waves clearly comes out in this approach. The characteristics retrieved from these plots agree well with theoretical predictions and previous observations, particularly regarding the discrete wave packet character of the Kelvin waves.

Together with the results from the spectral analysis, the time–height and time–latitude plots support the existence of Kelvin waves in discrete frequency bands, which do not vary much despite changing mean flow conditions. The comparison between period I and period II, where there is very little evidence of ultrafast waves, suggests that the ultrafast waves may not always be excited but do not undergo major frequency shifts depending on the background winds.

One of the interesting results of the analysis was the observed displacement of the wave peak off the equator, which was seen to increase with height, particularly during period I. It would be tempting to seek to explain this equatorial asymmetry as a response to the latitudinal shear of mean zonal flow. This is in contrast to theoretical studies by Boyd (1978a,b), which suggest that the slower Kelvin modes at least are not visibly influenced by latitudinal shear of the mean flow. On the other hand, it is well established, theoretically and experimentally, that vertical shears have a strong influence on these waves (Coy and Hitchman 1984). Figure 1a shows that above 5 hPa there exists an easterly vertical shear in the Southern (summer) Hemisphere, while in the Northern Hemisphere either there is practically no shear or it is slightly westerly or easterly depending on the height. On the other hand, during period II the stronger shears in the lower part of the region are basically equatorially symmetric, while in the region above 5 hPa, the easterly vertical shear in the summer hemisphere is reduced in comparison to period I. The wavenumber 1 components at this time show practically no sign of latitudinal displacement; only the wavenumber 2 components have some degree of asymmetry. In the latter case no increase of asymmetry with height is evident as, say, in Figs. 5a or 5c. This could imply the existence of a mechanism that locally amplifies or damps the propagating wave because of the differential wind shear.

For the Kelvin wave–induced perturbations in ozone, the change from a transport-dominated regime below 10 hPa to a photochemically controlled regime above 10 hPa was clearly apparent in the diagnosis of the MLS observations described in this paper. This altitude dependence in the character of the ozone perturbation was seen in the time–height plots, in the vertical structure of the power spectra, in the meridional cross sections, and in the height dependence of the phase difference between temperature and ozone.

The ratios of the ozone perturbation amplitude to the temperature perturbation amplitude for the various observed Kelvin wave modes is in agreement with model estimates and LIMS observations in the lower half of

the region sampled but appears to be larger in the upper stratosphere and lower mesosphere. This could be related to the fact that the maximum Kelvin wave–induced ozone perturbation in the region above the zonal mean mixing ratio peak tends to occur at a higher altitude than in the LIMS results.

Acknowledgments. The authors wish to thank Prof. C. Leovy, Prof. J. M. Wallace, and Dr. R. Lieberman for comments and discussions during the development of this paper. This research was supported by the *Upper Atmosphere Research Satellite* project under NASA Contract NAS5-26301.

REFERENCES

Barath, F. T., and coauthors, 1993: The Upper Atmosphere Research Satellite Microwave Limb Sounder. *J. Geophys. Res.*, **98,** 10 751–10 762.

Boyd, J., 1978a: The effects of latitudinal shear on equatorial waves. Part I: Theory and methods. *J. Atmos. Sci.*, **35,** 2236–2258.

——, 1978b: The effects of latitudinal shear on equatorial waves. Part II: Applications to the atmosphere. *J. Atmos. Sci.*, **35,** 2259–2267.

Chang, C., 1976: Forcing of stratospheric Kelvin waves by tropospheric heat sources. *J. Atmos. Sci.*, **35,** 740–744.

Coy, L., and M. Hitchman, 1984: Kelvin wave packets and flow acceleration: A comparison of modeling and observations. *J. Atmos. Sci.*, **41,** 1875–1880.

Elson, L., and L. Froidevaux, 1993: The use of Fourier transforms for asynoptic mapping: Applications to the Upper Atmosphere Research Satellite Microwave Limb Sounder. *J. Geophys. Res.*, **98,** 23 039–23 050.

Hayashi, Y., 1970: A theory of large-scale equatorial waves generated by condensation heat and accelerating the zonal wind. *J. Meteor. Soc. Japan,* **48,** 140–160.

Hirota, I., 1978: Equatorial waves in the upper stratosphere and mesosphere in relation to the semiannual oscillation of the zonal wind. *J. Atmos. Sci.*, **35,** 714–722.

——, 1979: Kelvin waves in the equatorial middle atmosphere observed with Nimbus 5 SCR. *J. Atmos. Sci.*, **36,** 217–222.

Hitchman, M. H., and C. B. Leovy, 1988: Estimation of the Kelvin wave contribution to the semiannual oscillation. *J. Atmos. Sci.*, **45,** 1462–1475.

Holton, J. R., 1970: The influence of mean wind shear on the propagation of Kelvin waves. *Tellus,* **22,** 186–193.

——, 1972: Waves in the equatorial stratosphere generated by tropospheric heat sources. *J. Atmos. Sci.*, **29,** 368–375.

——, 1973: On the frequency distribution of atmospheric Kelvin waves. *J. Atmos. Sci.*, **30,** 499–501.

——, 1992: *Introduction to Dynamic Meteorology.* 3d ed. Academic Press, 511 pp.

——, and R. S. Lindzen, 1968: A note on "Kelvin" waves in the atmosphere. *Mon. Wea. Rev.*, **96,** 385–386.

Lait, L. R., and J. L. Stanford, 1988: Applications of asynoptic space–time Fourier transform methods to scanning satellite measurements. *J. Atmos. Sci.*, **45,** 3784–3799.

Maruyama, T., 1969: Long-term behavior of Kelvin waves and mixed Rossby–gravity waves. *J. Meteor. Soc. Japan,* **47,** 245–254.

Randel, W. J., 1990: Kelvin wave–induced trace constituent oscillations in the equatorial stratosphere. *J. Geophys. Res.*, **95,** 18 641–18 652.

——, and J. C. Gille, 1991: Kelvin wave variability in the upper stratosphere observed in SBUV ozone data. *J. Atmos. Sci.*, **48,** 2336–2349.

Salby, M. L., 1982a: Sampling theory for asynoptic satellite observations. Part I: Space–time spectra, resolution, and aliasing. *J. Atmos. Sci.*, **39,** 2577–2600.

——, 1982b: Sampling theory for asynoptic satellite observations. Part II: Fast Fourier synoptic mapping. *J. Atmos. Sci.*, **39,** 2601–2614.

——, and R. R. Garcia, 1987: Transient response to localized episodic heating in the tropics. Part I: Excitation and short-time near-field behavior. *J. Atmos. Sci.*, **44,** 458–498.

——, D. L. Hartmann, P. L. Bailey, and J. C. Gille, 1984: Evidence for equatorial Kelvin modes in *Nimbus-7* LIMS. *J. Atmos. Sci.*, **41,** 220–235.

——, P. Callaghan, S. Solomon, and R. R. Garcia, 1990: Chemical fluctuations associated with vertically propagating equatorial Kelvin waves. *J. Geophys. Res.*, **95,** 20 491–20 505.

Stolarski, R. S., and A. R. Douglass, 1985: Parameterization of the photochemistry of stratospheric ozone including catalytic loss processes. *J. Geophys. Res.*, **90,** 10 709–10 718.

Sun, C., and C. Leovy, 1990: Ozone variability in the equatorial middle atmosphere. *J. Geophys. Res.*, **95,** 13 829–13 849.

Swinbank, R., and A. O'Neill, 1994: A stratosphere–troposphere data assimilation system. *Mon. Wea. Rev.*, **122,** 686–702.

Takahashi, M., and B. A. Boville, 1992: A three-dimensional simulation of the equatorial quasi-biennial oscillation. *J. Atmos. Sci.*, **49,** 1020–1035.

Wallace, J. M., and V. Kousky, 1968: Observational evidence of Kelvin waves in the tropical stratosphere. *J. Atmos. Sci.*, **25,** 900–907.

Waters, J. W., L. Froidevaux, W. G. Read, G. L. Manney, L. S. Elson, D. A. Flower, R. F. Jarnot, and R. S. Harwood, 1993: Stratospheric CLO and ozone from the Microwave Limb Sounder on the Upper Atmosphere Research Satellite. *Nature,* **362,** 597–602.